Test of hybrid panel in compression

NFFP-5, POSCOS

ROLF JARLÅS, JOAKIM SCHÖN, PER DAVIDSSON

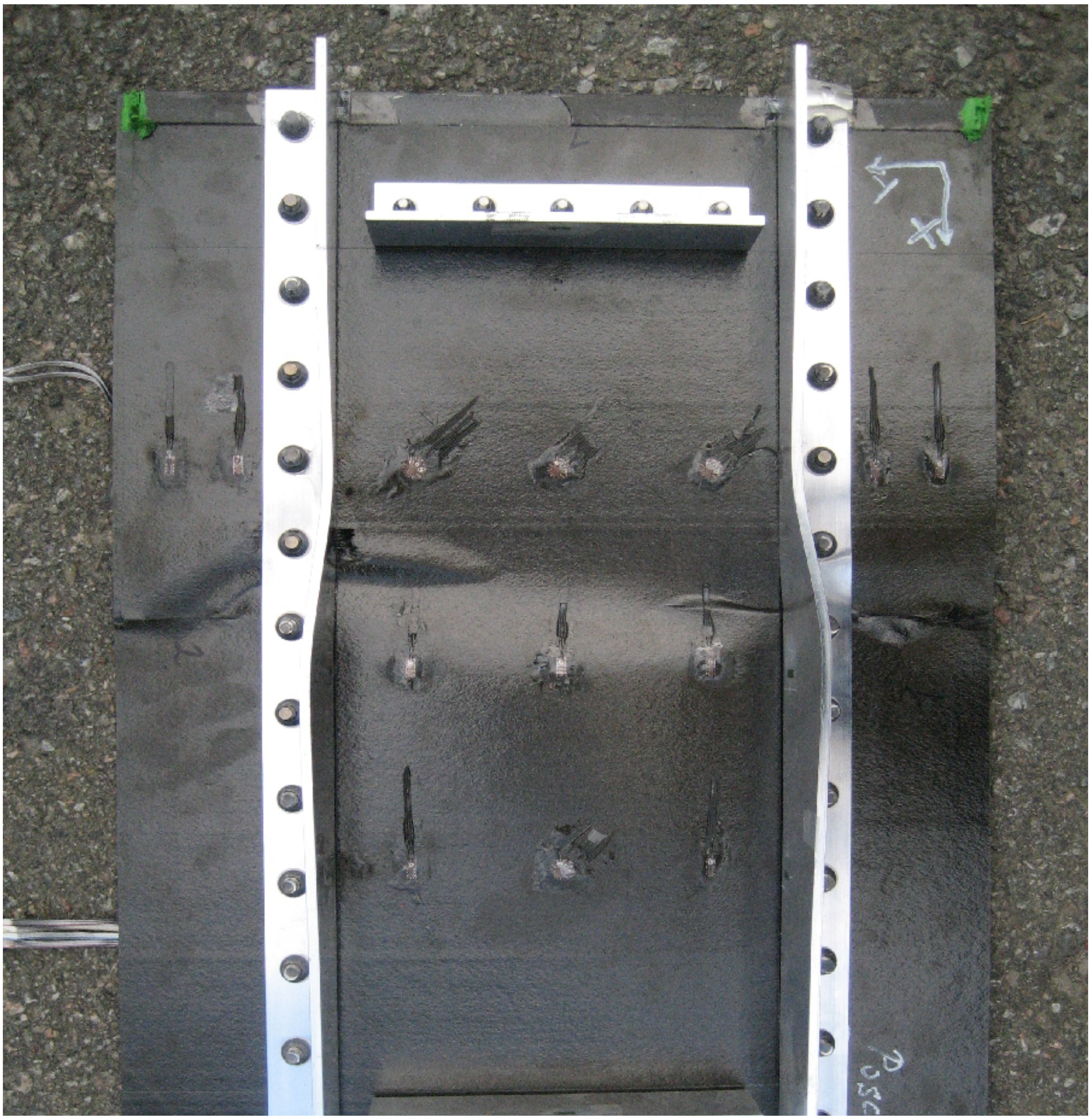

FOI-R--3843--SE
ISSN 1650-1942 January 2014

Rolf Jarlås, Joakim Schön, Per Davidsson

Test of hybrid panel in compression

NFFP-5, POSCOS

Bild/Cover: Collapsed specimen after successful test

Titel	Provning av hybrid panel belastad i tryck
Title	Test of hybrid panel in compression
Rapportnr/Report no	FOI-R—3843--SE
Månad/Month	Jan
Utgivningsår/Year	2014
Antal sidor/Pages	49 p
ISSN	1650-1942
Kund/Customer	SAAB (NFFP-5 Vinnova)
Forskningsområde	3. Flygteknik och luftstridssimulering
FoT-område	Flygteknik
Projektnr/Project no	E28216
Godkänd av/Approved by	Lars Höstbeck
Ansvarig avdelning	Informations- och aerosystem

Sammanfattning

Projektet POSCOS inom det nationella flygforskningsprogrammet (NFFP) syftar till metodutveckling gällande dimensionering av bucklingsbenägna kompositstrukturer.

I denna rapport presenteras provresultatet för en tryckbelastad hybridpanel med aluminium-förstyvningar som skruvats fast mot det plana kompositskinnet (POSCOS-1). Panelen tillverkades av SAAB AB och provningen genomfördes vid FOI. Provresultaten som beskrivs här innefattar såväl last-, töjnings- och fullfälts-mätning med det optiska systemet Aramis. Provningen visar att kollapslasten är cirka tre gånger högre än bucklingslasten för skinnet, samt att ett mindre antal lastcykler till nivåer avsevärt högre än bucklingslasten kan göras utan att medföra några observerbara skador eller mätbara rest-töjningar.

Provresultaten kan jämföras med motsvarande prov för en integral svagt enkelkrökt kompositpanel (POSCOS-2).

Nyckelord:

komposit, panel, hybrid struktur, buckling, prov, test, tryck

Summary

The project POSCOS within the Swedish National Aeronautical Research program (NFFP) aims at method development regarding strength prediction and sizing-methods for buckling-critical composite structures. The test results are reported for a panel where aluminium-stringers are bolted to the flat composite skin (POSCOS-1) loaded in compression. The panel was produced by SAAB AB, and the testing was performed at FOI. The test-results contain load-, strain and full-field measurements using the optical system Aramis. The measurement shows that the collapse load is approximately three times higher than the buckling load for the skin. It is also found that a limited number of load-cycles well above the buckling load do not cause any observable damage or measurable residual strain.

These results can be compared with those for a similar test performed on an integrally stiffened slightly curved composite panel (POSCOS-2).

Keywords: composite, panel, integral panel, buckling, test, compression

Contents

1 Introduction

Composites are often used to reduce weight in aircraft structures. Some structures, or part of structures, will be subjected to compressive loading and as a result buckling might occur. For such cases the buckling load is often the factor that drives the design. Buckling in composite structures is not allowed at operational loads. Allowing it would enable a considerable reduction in weight. Considerable work has been done in the past on buckling of monolithic structures made of aluminium. There are handbooks on how to estimate the buckling load and numerical methods have been verified. A large number of experiments have been done in the past. Composites are orthotropic and equations for monolithic materials are not necessarily valid. Therefore, numerical methods and handbook methods need to be developed for composites. That has been done in another part of the project. Those methods need to be validated against experiments and this report describes such an experiment.

The objective of the investigation has been to determine the buckling displacement shape for a hybrid composite panel with composite skin and aluminium stringers. Strain gauges are attached at several points to measure strain and strain redistribution due to nonlinear effects, with high accuracy and to determine the load required to cause subsequent residual strain. To determine the compressive failure load of the specimen is also included as an objective. The panel was produced by SAAB AB, and the testing was performed at FOI.

2 Experimental procedure

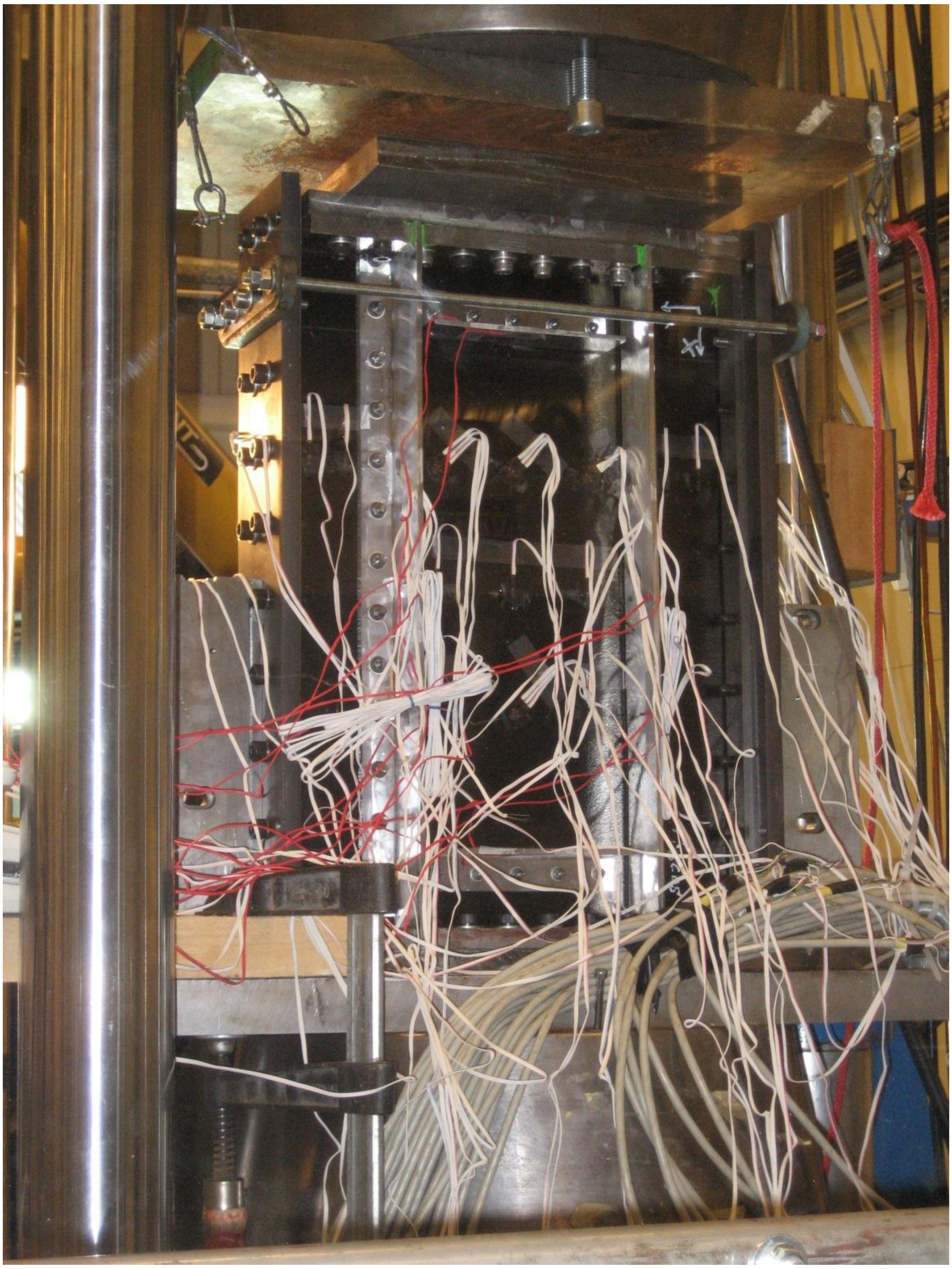

Figure. 2.1 Specimen with strain gauges mounted in the test rig

2.1 Test rig and boundary conditions

The specimen was mounted in a test rig, see Fig. 2.1. The lower and upper edge of the specimen was placed on wide thick flat steel plates. Around the lower and upper sides of the specimen edges there were smaller 20 mm thick steel plates, mounted with bolts to the wide flat plates. The tracks formed between the smaller steel plates were about 8-10 mm wider than the thickness of skin and stiffener. These tracks were completely filled with epoxy to obtain clamped conditions at the lower and upper edges of the panel. The upper steel plate was guided by the rig and movable vertically, following the stroke in a load frame. The two straight vertical edges of the panel were mounted without applying pressure between straight adjustable steel rulers with sharp edges to obtain simple support conditions.

To apply the compressive loading on the specimen the rig was placed on top of the lower grip in a MTS hydraulic testing machine with a capacity of 1000 kN. The lower grip was moved upward until contact was made with the upper grip and compression could be applied, see Fig. 2.2. The applied force and grip displacement were measured with the sensors in the load frame.

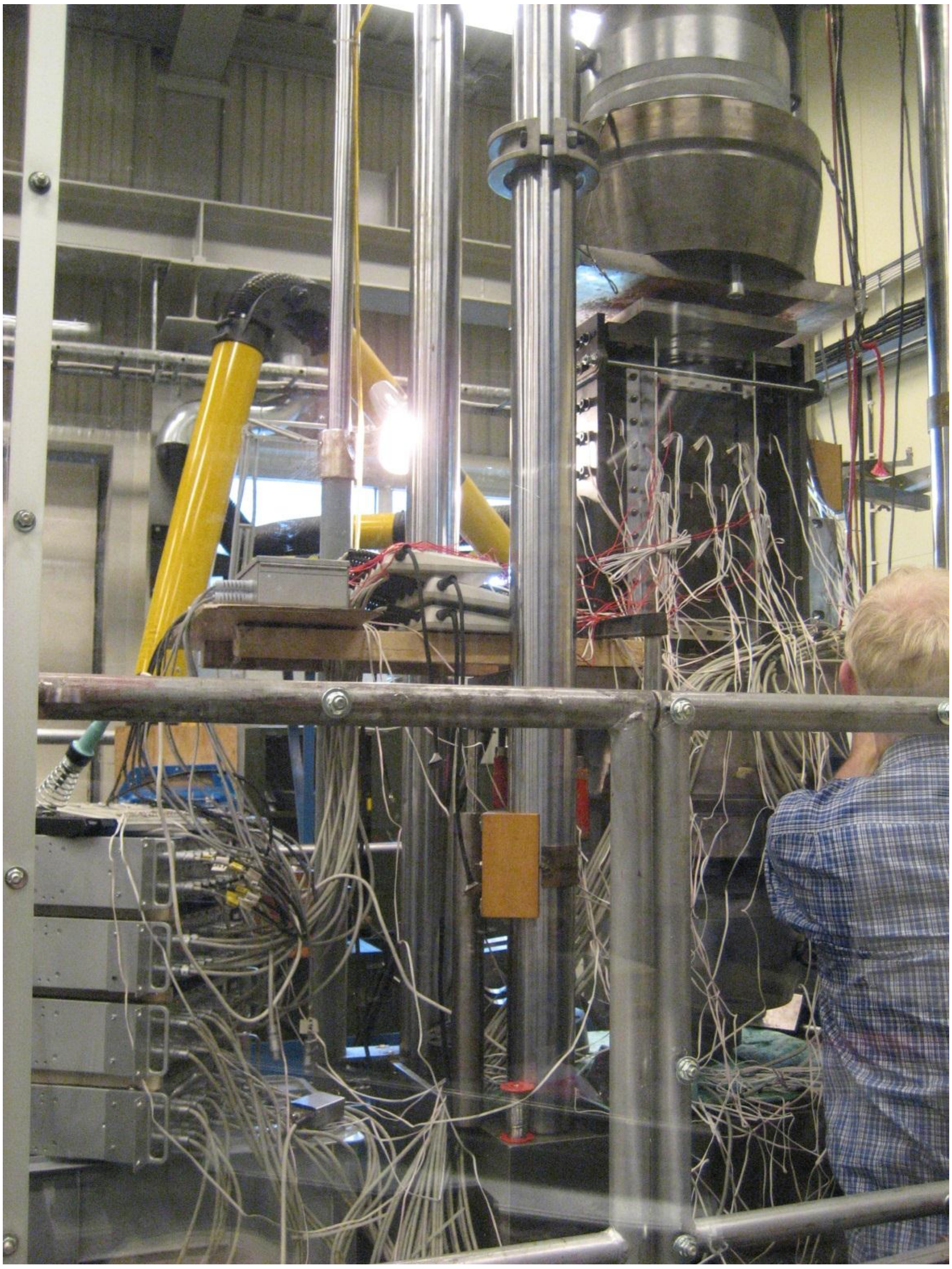

Figure. 2.2 Specimen mounted in the test rig and load frame

2.2 Panel geometry

The panel illustrated in Fig. 2.3 has a flat skin with a width of 400 mm and height 580 mm. Nominal skin thickness is 3.12 mm. Two long vertical L-shaped aluminium stringers are bolted to the skin. Fourteen 8 mm bolts in a single row are used for each stringer. The stringer-height is 60 mm, and stringer foot width is 32.5 mm, with a thickness of 4.5 mm. The distance between the free webs is 200 mm.

There are short (170 mm) horizontal rib-foots between the stringers close to the upper and lower horizontal edges of the panel. These rib-foots are L-shaped, with a thickness of 4.5 mm, a height of 44.5 mm and a flange width of 32.5 mm. These profiles are bolted with 6 mm bolts to the skin.

A straight ruler was used to find any visible waviness in the skin. The panel was found to be everywhere straight on the stringer-free side of the skin.

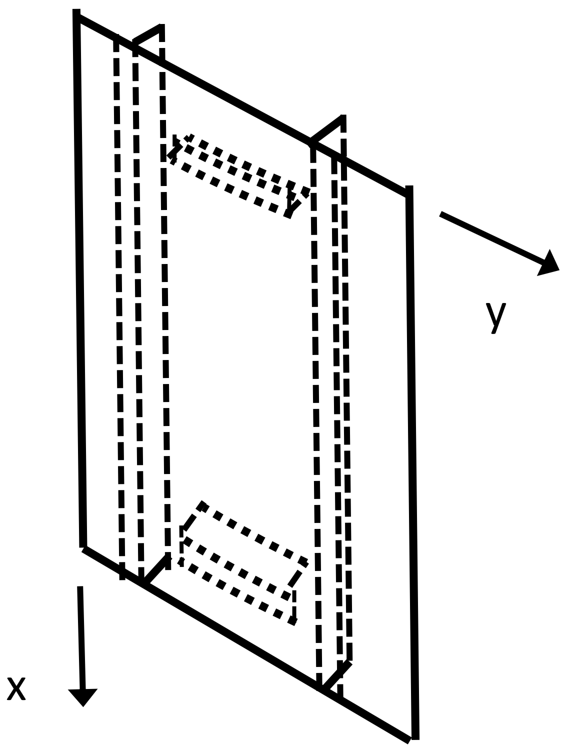

Figure. 2.3 Panel design principle

2.3 Panel material properties and layup

The composite skin is close to quasi-isotropic but with a reduced number of +/-45^{o} plies. The composite properties for the skin are summarized in Tab. 2.1, with reference to SAAB for more detailed questions. Typical aluminium stringer properties are given for comparison.

Table 2.1 Composite properties

	Skin	**Stringer**
% 0^o	33.3	
% 45^o	33.4	
% 90^o	33.3	
E_{11} (MPa)	60783	71000
E_{22} (MPa)	60783	
G_{12} (MPa)	15233	
G_{13} (MPa)	5190	
ν_{12}	0.2052	0.3

2.4 Load sequence

During loading of the specimen the displacement of the grip was controlled. The load sequence is schematically illustrated in Fig. 2.4. The coordinate system was adjusted such that zero was when the rig made contact with the upper grip. Before testing begun the lower grip was moved such that it was 0.2 mm below zero, the rig was not in contact with the upper grip. The specimen was then loaded at 1 mm/min rate until the first prescribed maximum stroke was reached where it was hold for 15 s. It was then unloaded at 1 mm/min until the stroke reached -0.2 mm and the specimen rig was not in contact with the upper grip. The procedure was then repeated one more time with a larger maximum stroke. The maximum stroke was then increased for the next set of two cycles. During the two displacement cycles all signals measured was recorded and stored. Data from the measurements were gathered in blocks, called Log, where each Log typically contains data for two load-cycles. The relation between Log number, cycle number, maximum stroke and maximum load is presented in Table 2.2.

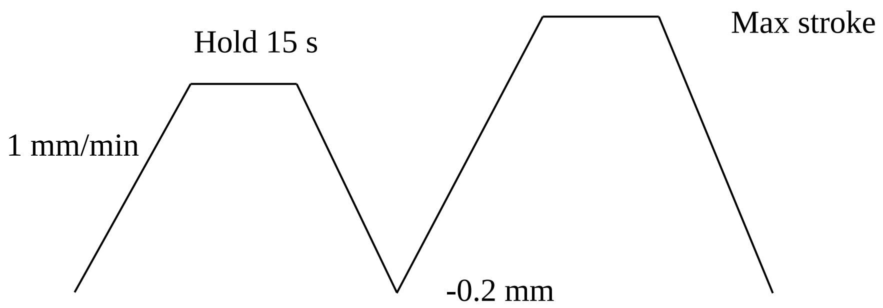

Figure. 2.4 Schematic of displacement controlled test cycle

Table 2.2 Load sequence and Log-numbers

*)Remark: In Log 1-Log 23 the grips in the testing-machine was not perfectly fixed and max Stroke is not consistent with values measured until from Log 25.

Log No.	**Cycle**	**max Stroke (mm)**	**max Load (kN)**	**Remark**
1	1	0.4*	8	
	2	0.6*	20	
3	1	0.4*	8	
	2	0.6*	21	
5	1	0.8*	37	
	2	1.0*	56	
7	1	1.2*	73	
	2	1.4*	87	
9	1	1.6*	96	
	2	1.7*	100	Safety stop at 100 kN, about 1.7 mm
11	1	1.8*	98	
	2	2.0*	101	
13	1	2.2*	104	
	2	2.4*	105	Insufficient fixation of the grips caused flexing. Ten (10) cycles with maximum load in the range 100-125 kN was made before a solution with fixation was introduced. First tested in Log 25
25	1	1.4		
26	1	1.4	124	
	2	1.6	154	
27	1	1.8	180	
	2	?	197	Security stop
29	1	2.0	203	

	2	2.2	228	
31	1	2.4	253	
	2	2.6	277	First noise (low short)
33	1	2.8	300	
	2	3.0	330	
35	1	3.2	354	
	2	3.4	378	Noise near 340-350 kN during loading and at 320 kN when unloading
37	1	3.6	400	Noise at 340 kN during loading. Also heard in the following cycles
	2	3.8?		Control-computer related stop
38	1	3.8	429	
	2	4.0	449	Hysteresis in strain results. Peak, 4600 μStrain correspond to 327 MPa in stringer at gauge 46. Noise perhaps indicating some damage growth
40	1	4.2	465	Severe hysteresis in strain response
	2	4.4	485	
42	1	4.6	493	Noise indicating damage growth near 490 kN
	2	4.8	499	Noise indicating damage growth near maximum load
44	1	5.0*	495	*Structural failure across entire panel, not far from middle (X=290)

2.5 Strain gauge measurements

A total of 62 strain-gauges were used, located as illustrated in Fig. 2.5. Their coordinates are given in Table 2.3. Gauges were attached on both sides of the composite skin and on the stringers to make it possible to determine membrane- and bending strains, to monitor load redistribution due to buckling, and to determine when buckling occurs. The gauges measuring strain in the direction of the applied load (X) were located at three different X-coordinates (190, 290 and 390 mm) from the top of the panel. This means that the second row of gauges were on the line of symmetry for the panel. There were three columns with gauges between the stringers. With nominal values these were at Y=133, 200 and 267 mm, and two columns outside of each stringer at Y=28.5, 58.5, 341.5 and 371.5 mm[1] (Notice that these Y-coordinates differ compared to the integral panel due to the stringer-foot on the hybrid panel). To get an indication of bending and lifting of the stringer web from the skin there were 12 gauges measuring strain in the Z-direction on the stringers.

The strain gauges were excited with 2 V or 5 V and the change in resistance was measured with FFA bridge amplifiers. The strain gauges were connected to a Wheatstone bridge with two wires. The amplifiers used a fixed gain of 50 or 100 times. The strain was calculated directly in the data acquisition system based on the gauge factor and amplifier gain. In addition a shunt calibration with 10 kOhm resistance was done but not used in calculating strain.

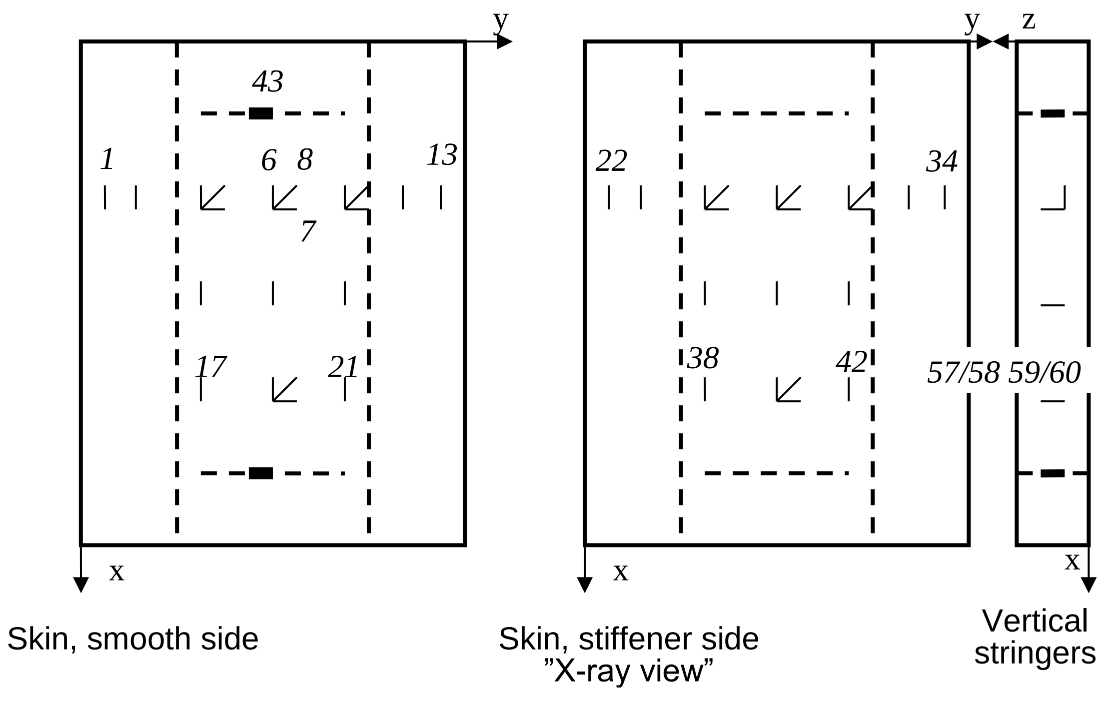

Figure 2.5 Illustration of strain-gauge positions and orientation. Numbering from left to right, top to bottom, smooth side then stiffener side. (Orientation of rosette diagonal may be 90^{o}-different from illustration)

[1] Remark:Poscos-2 had gauges 2,12,23 and 33 moved closer together because there was no stringer foot. The rosettes were oriented differently for practical reasons and measures 45 instead of -45 degrees in Poscos-2.

Table 2.3 strain gauge positions for the hybrid panel

(Measured positions, for plate measured to be 402 mm wide.

F=smooth side, B=stiffener side, S=stiffener or stringer, D=direction measured,

z=distance to skin on stiffener side)

No.	Skin smooth side	No.	Skin stiffener side	No.	Upper rib-foot
1	Fx=190, y=28.5, D=x	22	Bx=190, y=28.5, D=x	43	Sx=75.5, y=201, z=35, D=y
2	Fx=190, y=58.5, D=x	23	Bx=190, y=58.5, D=x	44	Sx=80, y=201, z=35, D=y
				No.	Long vertical stringers
3	Fx=190, y=134, D=x	24	Bx=190, y=134, D=x		
4	Fx=190, y=134, D=y	25	Bx=190, y=134, D=y	45	Sx=190, y=96.5, z=15, D=z
5	Fx=190, y=134, D=x,y	26	Bx=190, y=134, D=x,y	46	Sx=190, y=96.5, z=15, D=x
6	Fx=190, y=201, D=x	27	Bx=190, y=201, D=x	47	Sx=190, y=101, z=15, D=z
7	Fx=190, y=201, D=y	28	Bx=190, y=201, D=y	48	Sx=190, y=101, z=15, D=x
8	Fx=190, y=201, D=x,y	29	Bx=190, y=201, D=x,y	49	Sx=190, y=301, z=15, D=z
9	Fx=190, y=268, D=x	30	Bx=190, y=268, D=x	50	Sx=190, y=301, z=15, D=x
10	Fx=190, y=268, D=y	31	Bx=190, y=268, D=y	51	Sx=190, y=305.5, z=15, D=z
11	Fx=190, y=268, D=x,y	32	Bx=190, y=268, D=x,y	52	Sx=190, y=305.5, z=15, D=x
12	Fx=190, y=343.5, D=x	33	Bx=190, y=343.5, D=x	53	Sx=290, y=96.5, z=15, D=z
13	Fx=190, y=373.5, D=x	34	Bx=190, y=373.5, D=x	54	Sx=290, y=101, z=15, D=z
14	Fx=290, y=134, D=x	35	Bx=290, y=134, D=x	55	Sx=290, y=301, z=15, D=z
15	Fx=290, y=201, D=x	36	Bx=290, y=201, D=x	56	Sx=290, y=305.5, z=15, D=z
16	Fx=290, y=268, D=x	37	Bx=290, y=268, D=x	57	Sx=390, y=96.5, z=15, D=z
17	Fx=390, y=134, D=x	38	Bx=390, y=134, D=x	58	Sx=390, y=101, z=15, D=z
18	Fx=390, y=201, D=x	39	Bx=390, y=201, D=x	59	Sx=390, y=301, z=15, D=z
19	Fx=390, y=201, D=y	40	Bx=390, y=201, D=y	60	Sx=390, y=305.5, z=15, D=z
20	Fx=390, y=201, D=x,y	41	Bx=390, y=201, D=x,y	No.	Lower rib-foot
21	Fx=390, y=268, D=x	42	Bx=390, y=268, D=x	61	Sx=500, y=201, z=35, D=y
				62	Sx=504.5, y=201, z=35, D=y

2.6 Speckle photography, (Aramis)

The skin smooth side of the specimen was spray painted black and then a white colour was sputtered onto the surface to create a speckle pattern (a random irregular pattern of dots). A picture of the surface can be seen in Fig. 2.6. Two cameras were placed about 625 mm from the surface a distance 308 mm apart, see Fig 2.6. The camera angle is 25^{o}. This gives a measurements area of approximately 500x420 mm^2. Depth of focus was large due to a large aperture for the lenses. Pictures of the specimen were taken before loading and then every fifth or tenth second until the load cycle was finished. Since the maximum compressive load was kept constant for 15 seconds, at least one picture was always taken at the maximum compressive load. The pictures were analysed with Aramis commercial software. The origo in the Aramis system is approximately at the central strain gauge, x=290 mm and y=200 mm in the specimen coordinate system.

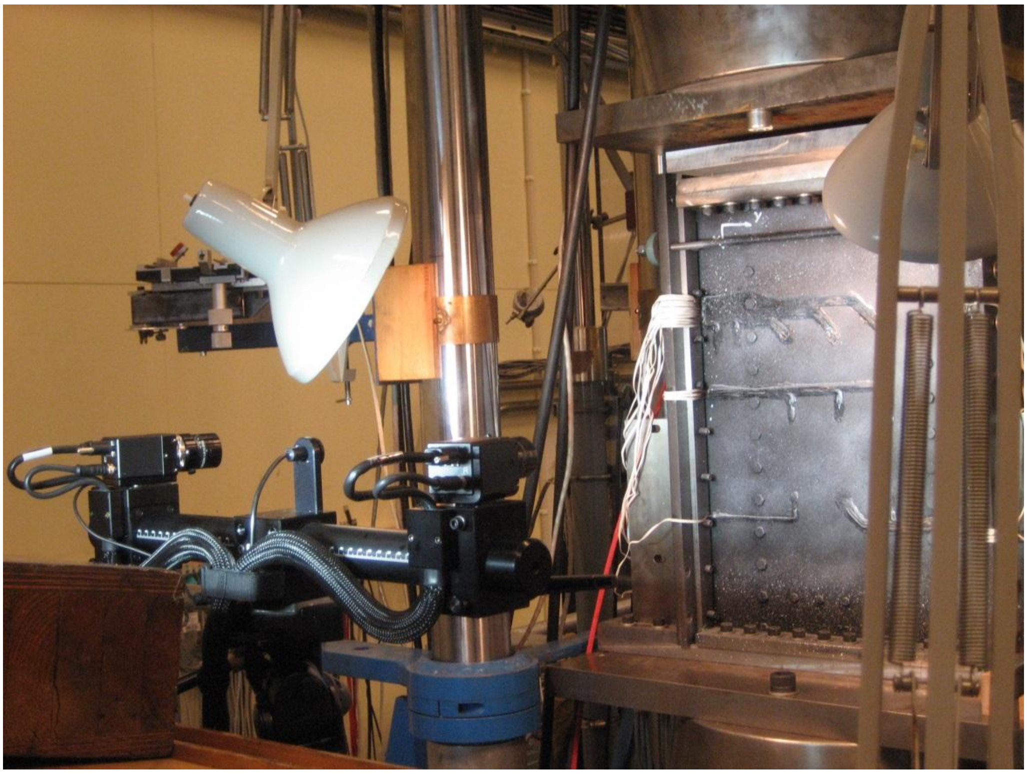

Figure. 2.6 Aramis cameras and specimen with speckle dots

A photo taken by the camera to the right as reference for Log 42 is shown in Fig. 2.7. A green region marks where Aramis will be able to evaluate displacements if the same region is also green on the corresponding picture from the left camera. A pair of reference photos are taken before loading starts for each Log.

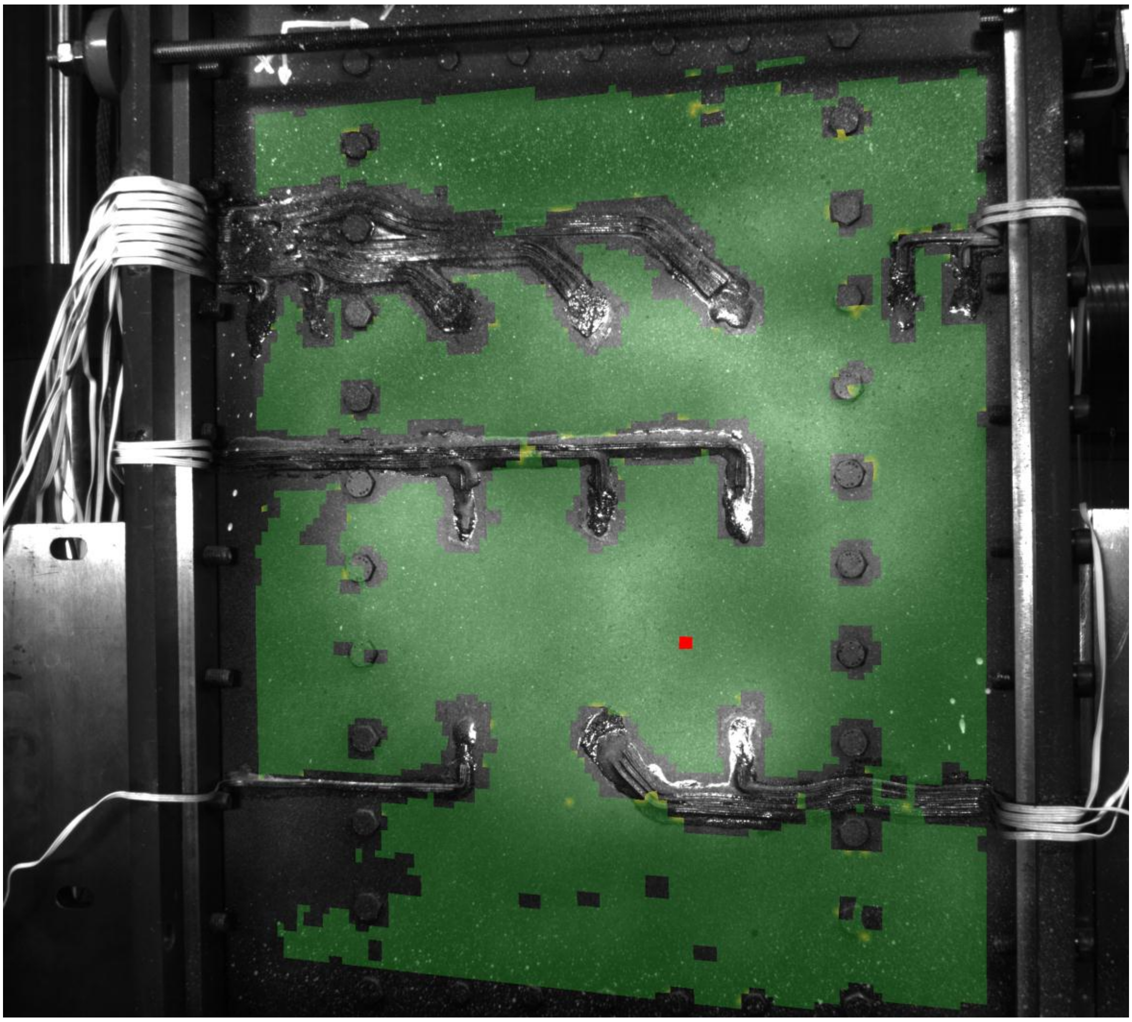

Figure 2.7 Photo taken by the camera to the right as reference for Log 42. The green region marks where Aramis will be able to evaluate displacements, if the same region is also green on the corresponding picture from the left camera

3 Results

During loading a compressive force was applied to the specimen. To show compressive forces, compressive strains and compressive grip displacement as positive the measured values have been scaled by -1 before being shown in figures.

3.1 Stroke response during load cycles

The grip displacement shown in Fig. 3.1 is measured with the transducer in the load frame. It is the same signal which is used by the controller and therefore it behaves well. At maximum stroke the displacement is kept constant for 15 s, which may be seen in Figure 3.1. Due to elastic deformation the grip displacement is probably larger than the actual displacement of the specimen. Most results will for this reason be presented as a function of the applied load, as measured by the load cell in the testing machine.

Figure 3.2 shows load as a function of grip displacement for Log 44 when the specimen breaks. The loading curve is slightly nonlinear shortly before failure the load does not increase although the grip displacement increases. At failure the load drops more than 200 kN.

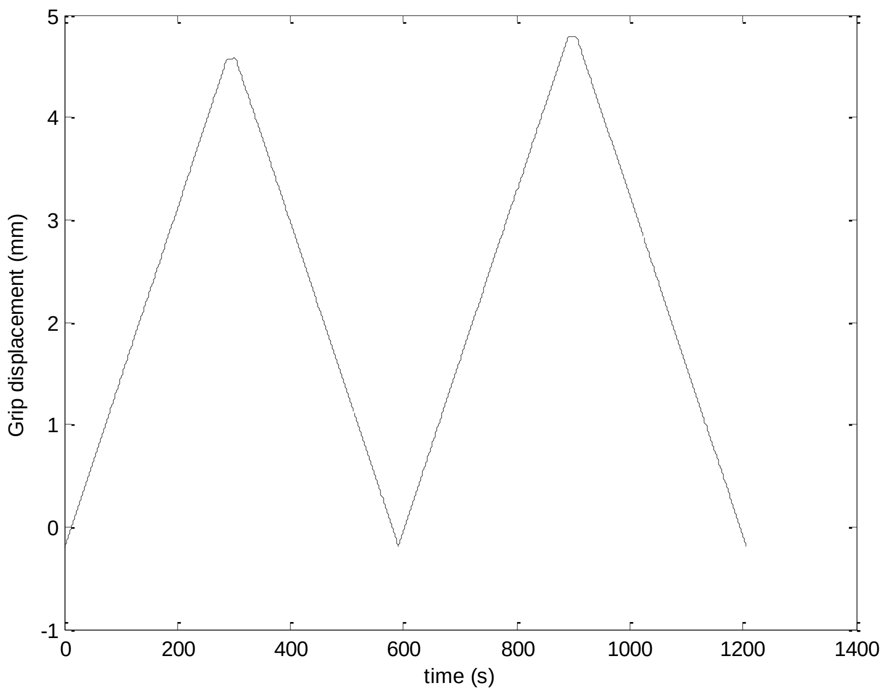

Figure. 3.1 Grip displacement from Log 42

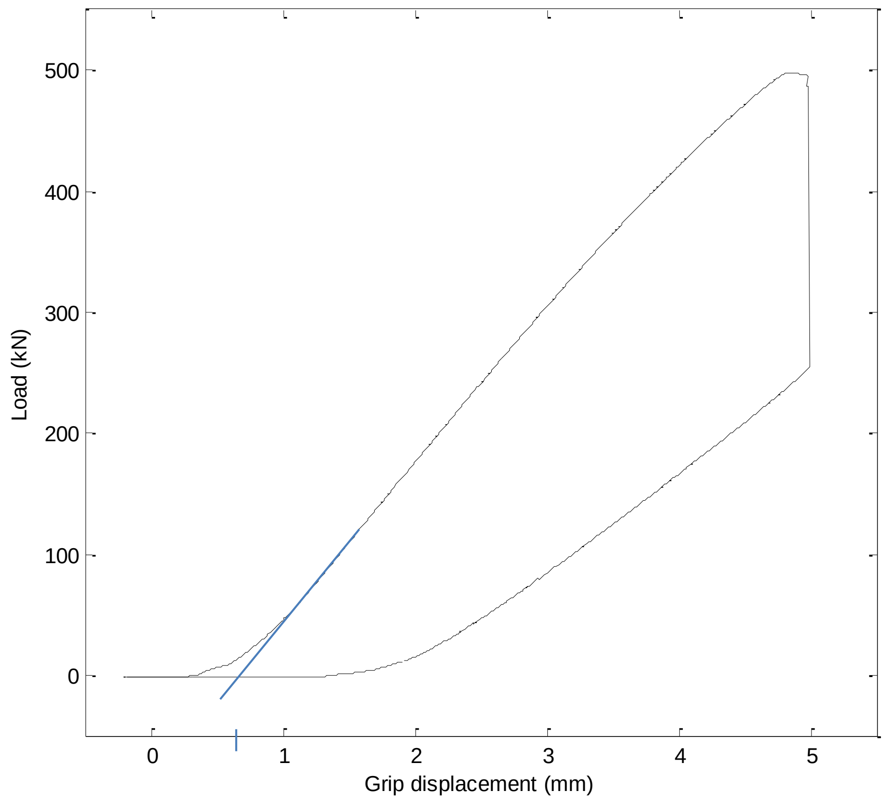

Figure. 3.2 Load versus grip displacement for Log 44 when specimen fails

3.2 Aramis measurements

The out of plane displacement as measured by the Aramis-system is shown at a load of 250 kN in Figs. 3.3&3.4 using different scales. As may be seen the system fails to measure displacements where the vires from the strain-gauges are attached. The bolt-heads for the stringers are also causing similar white regions. Looking at the displacement pattern in Fig. 3.3 it is seen that three large buckles have been formed, and that the one in the middle moves away from the cameras, while the other two moves toward the camera. That the buckle in the middle is concave when looking from the cameras is in agreement with the strain measurements (Fig. 3.16) showing that gauge 15 is on the more compressive side of the skin. Similarly gauges 6 and 18 which are on the convex side of the buckles measure tensile strain at 250 kN. The maximum amplitude in these buckles seems to be about -3.5 mm in the middle of the panel and slightly above +3.5 mm for the other two buckles. In Figure 3.4 it can be seen that outside of the stringers there is a small difference in displacement between the left and right side.

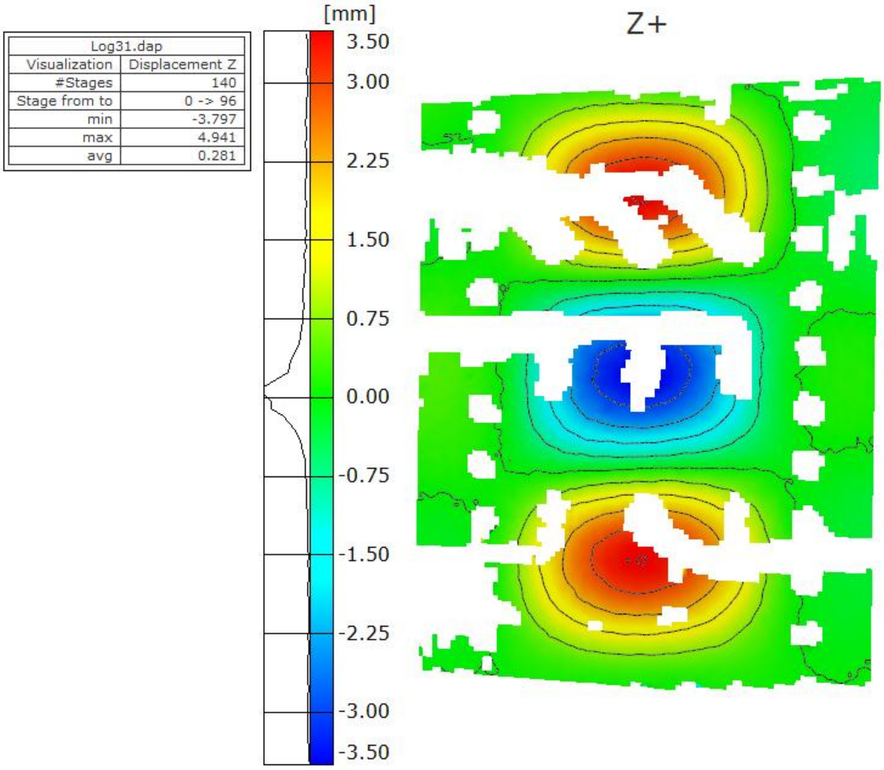

Fig. 3.3 Log 31, 250 kN cycle 2, 482 s (Loading). Out of plane displ. range [-3.5, +3.5] mm

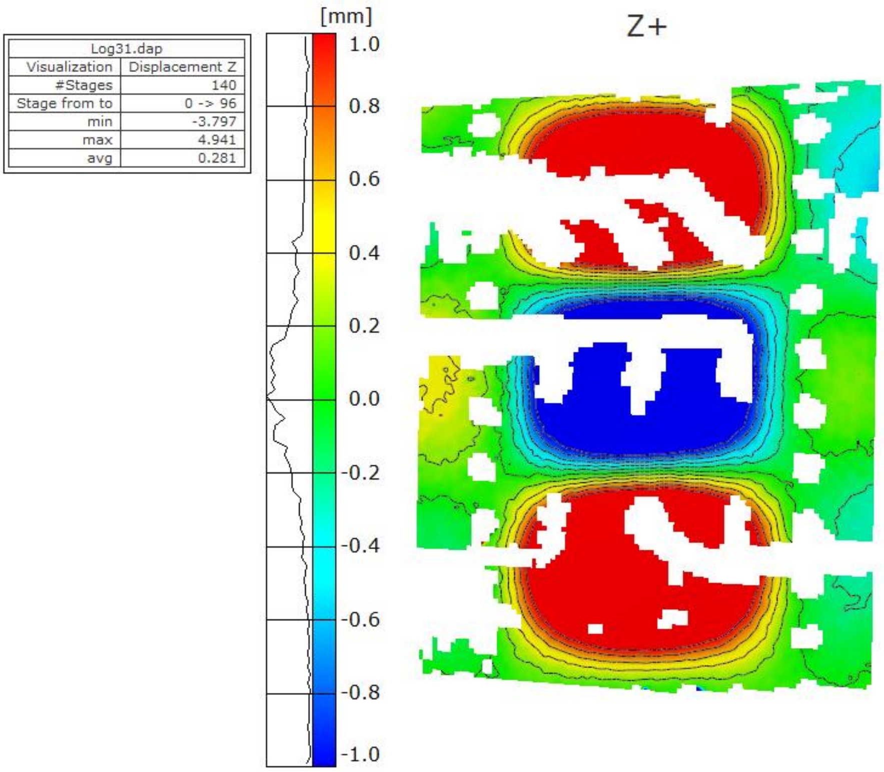

Fig. 3.4 Log 31, 250 kN, cycle 2 482 s (Loading). Out of plane displ. range [-1.,+1.] mm

The measured vertical displacement at 250 kN can be seen in Fig. 3.5. A small difference between left and right side is visible.

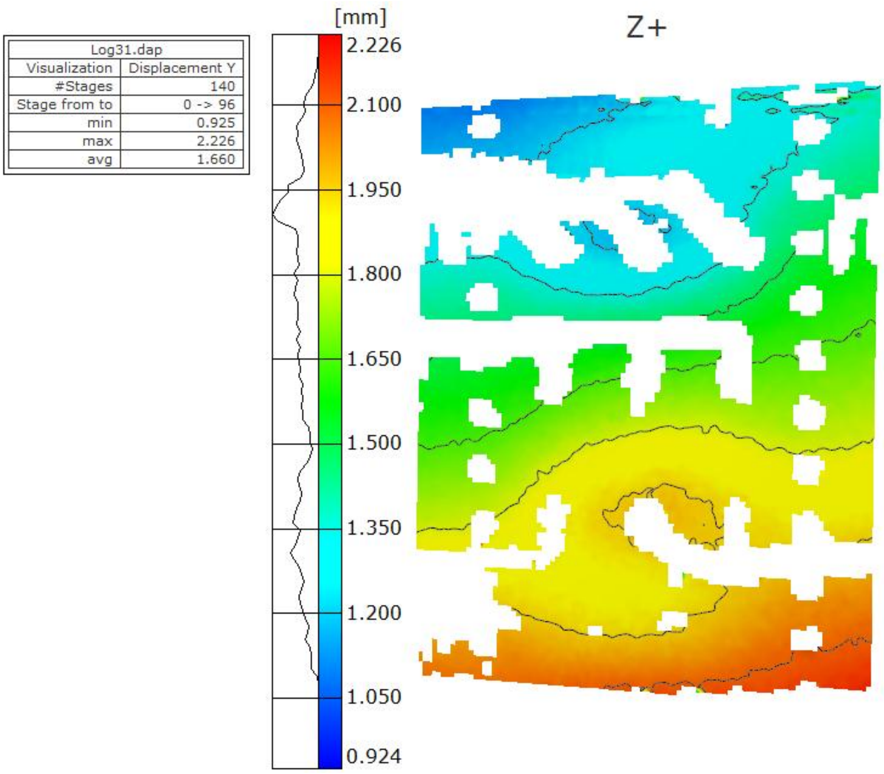

Figure. 3.5 Log 31 cycle 2, 482 sec, 250 kN (Loading) , Vertical displacement

The out of plane displacement at 400 kN are shown in Figs. 3.6 & 3.7. The minimum and maximum displacement measured are -5.62 and +5.91 mm respectively. The general shape is similar to that in Fig. 3.3.

In Figure 3.7 it is seen that the out of plane displacement outside of the stringers is related to the buckling shape between the stringers. The buckles on the outsides of the stringers are pointing in the opposite direction to the nearest buckle between the stringers.

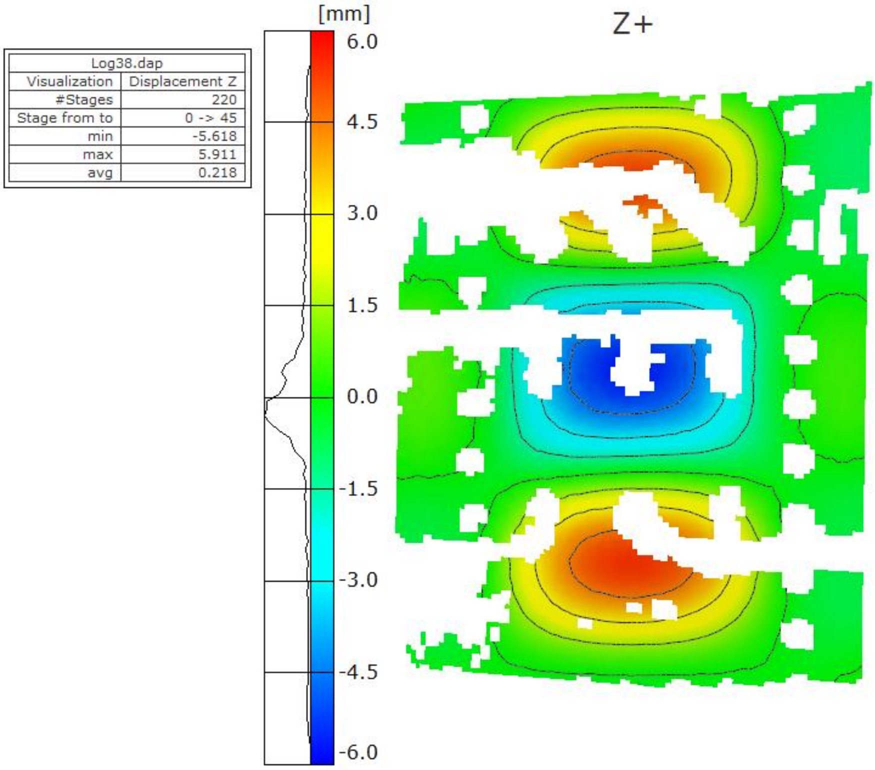

Fig. 3.6 Log 38, cycle 1, 227 s, 400 kN (Loading), Out of plane displ. range [-6.,+6.] mm

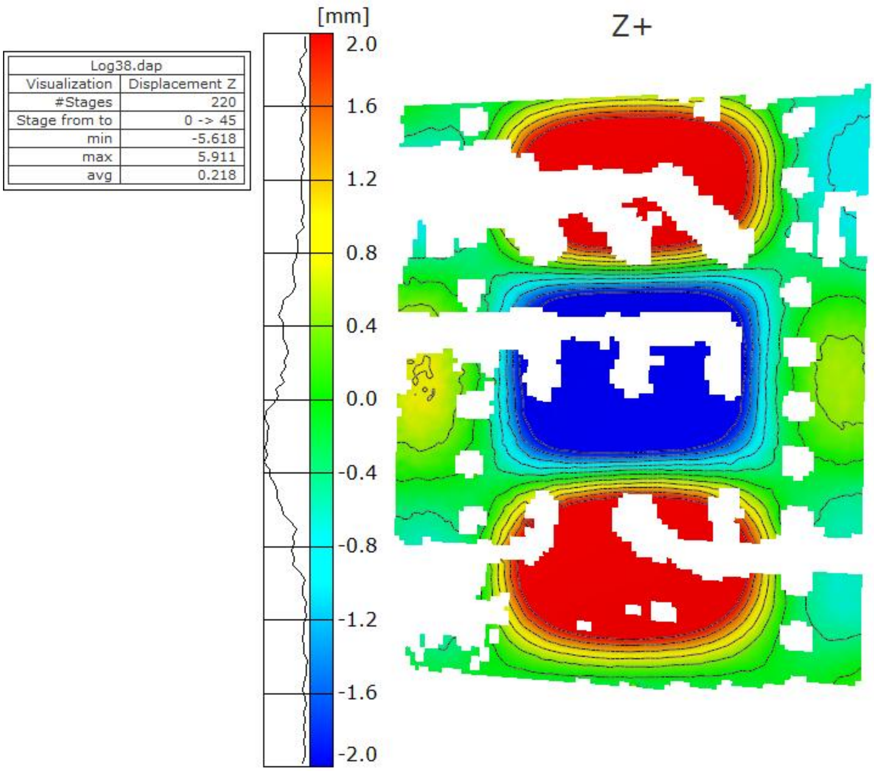

Fig. 3.7 Log 38, cycle 1, 227 s, 400 kN (Loading), Out of plane displ. range [-2.,+2.] mm

The vertical displacement at 400 kN is shown in Fig. 3.8. The difference in displacement between the upper and lower edge of the region photographed by Aramis is about 1.6 mm (3.1-1.5) at 400 kN, over a length of about 400 mm. Hence, an average strain of 0.4%. With a linear scaling to the full length of the panel the stroke would be 2.3 mm. The corresponding stroke measurement according to Tab. 2.2 is 3.6 mm..

Similar pictures as those shown here in Figs. 3.6-3.8 for Log 38 cycle 1 during loading at 400 kN were also produced for the other three instants when passing 400 kN in Log 38. Visually there are virtually no difference when comparing to the pictures above.

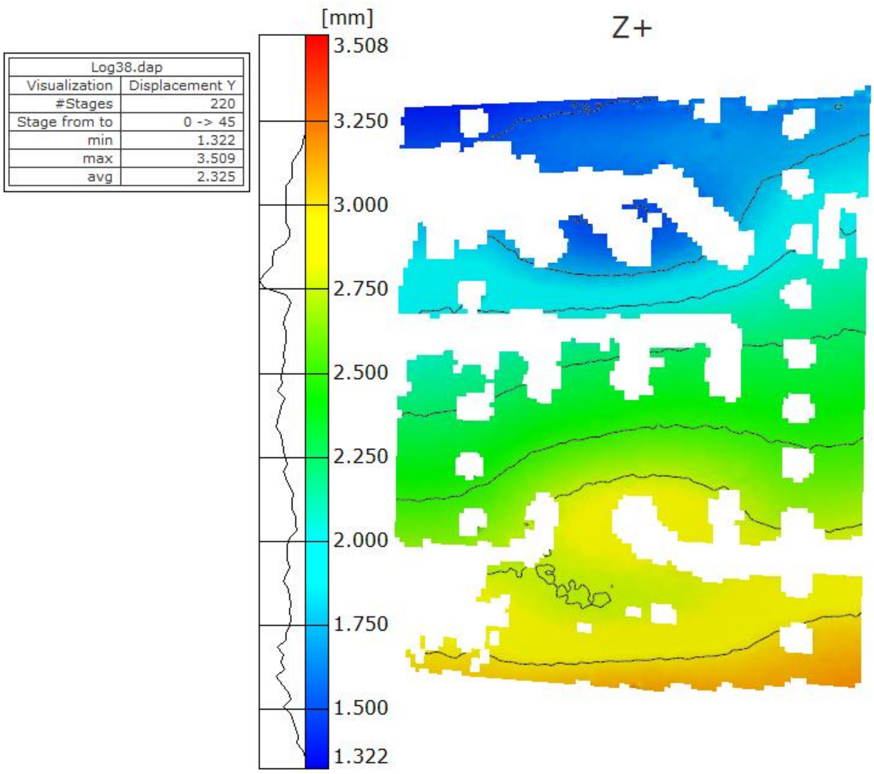

Figure. 3.8 Log 38 cycle 1, 227 s, 400 kN (Loading). Vertical displacement

The out of plane displacement at 490 kN during cycle 1 in Log 42 are shown in Figs. 3.9 & 3.10. The minimum and maximum displacement measured are -6.11 and +6.36 mm respectively. Compared to Figures 3.6-3.8 it is now at this higher load possible to see the lower part of a buckle at the upper part of the visible region between the stringers. The other three buckles have moved a bit downward.

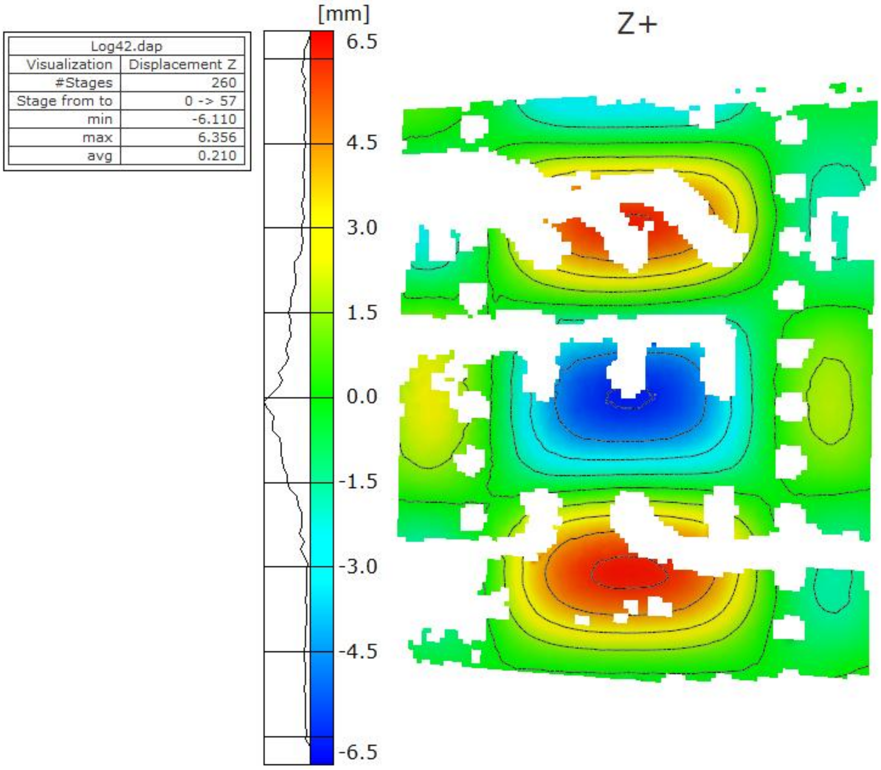

Figure. 3.9 Log 42 cycle 1, 286 s, 490 kN (Loading), Out of plane displacement range [-6.5,+6.5] mm

Comparing Log 42 cycle 1 at 490 kN during loading in Fig. 3.9 with the corresponding picture for cycle 2, at the same load and also during loading, it is only one very small detail that perhaps could be of importance; the blue area at the top of the picture in Fig. 3.10 is slightly bigger than in Fig. 3.9. If this is caused by some permanent deformation of the panel, or if it is due to small differences in measurements and applied load when the pictures was taken is not possible to say. A similar growth of the blue area at the top is seen when comparing Figure 3.11 and Figure 3.10, where Figure 3.11 is from the loading in cycle 1 of Log 44 at 490 kN.

There is a risk that the extreme displacements registred by Aramis originate from a (very local) point where the measurements are in error. The displacement values at 490 kN are given explicitly in Table 3.1.

Table 3.1 Out of plane extreme values at 490 kN

Log No.	**Cycle**	***Uz*-min (mm)**	***Uz*-max (mm)**	**Difference (mm)**
42	1 up	-6.11	6.36	12.47
42	2 up	-5.93	6.40	12.33
44	1 up	-5.29	6.58	11.87

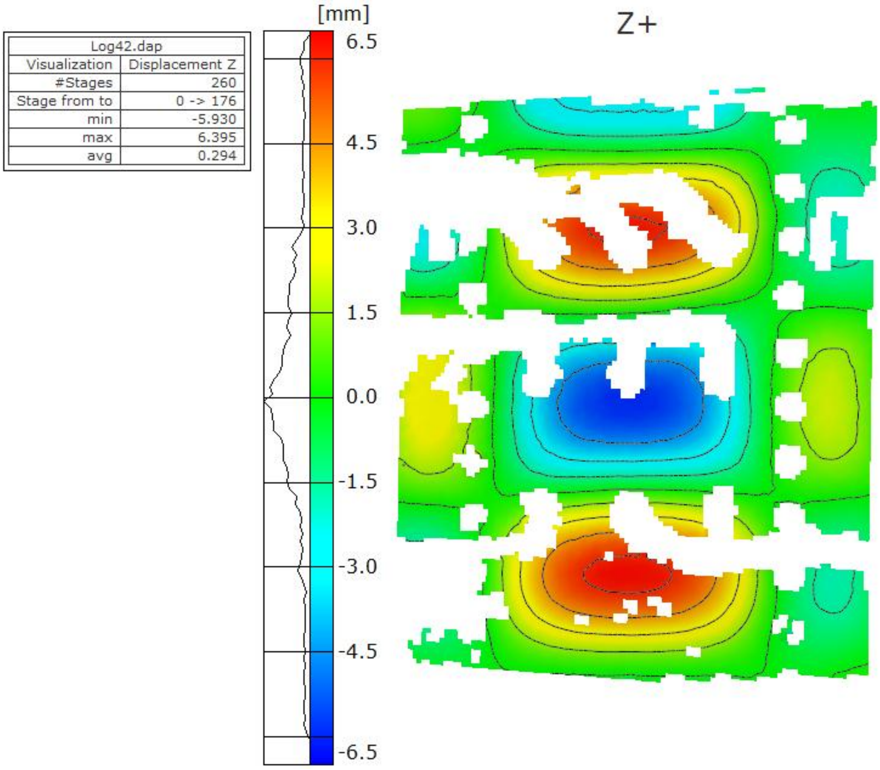

Fig.. 3.10 Log 42 cycle 2, 879 s, 490 kN (Loading), Out of plane displ. range [-6.5,+6.5] mm

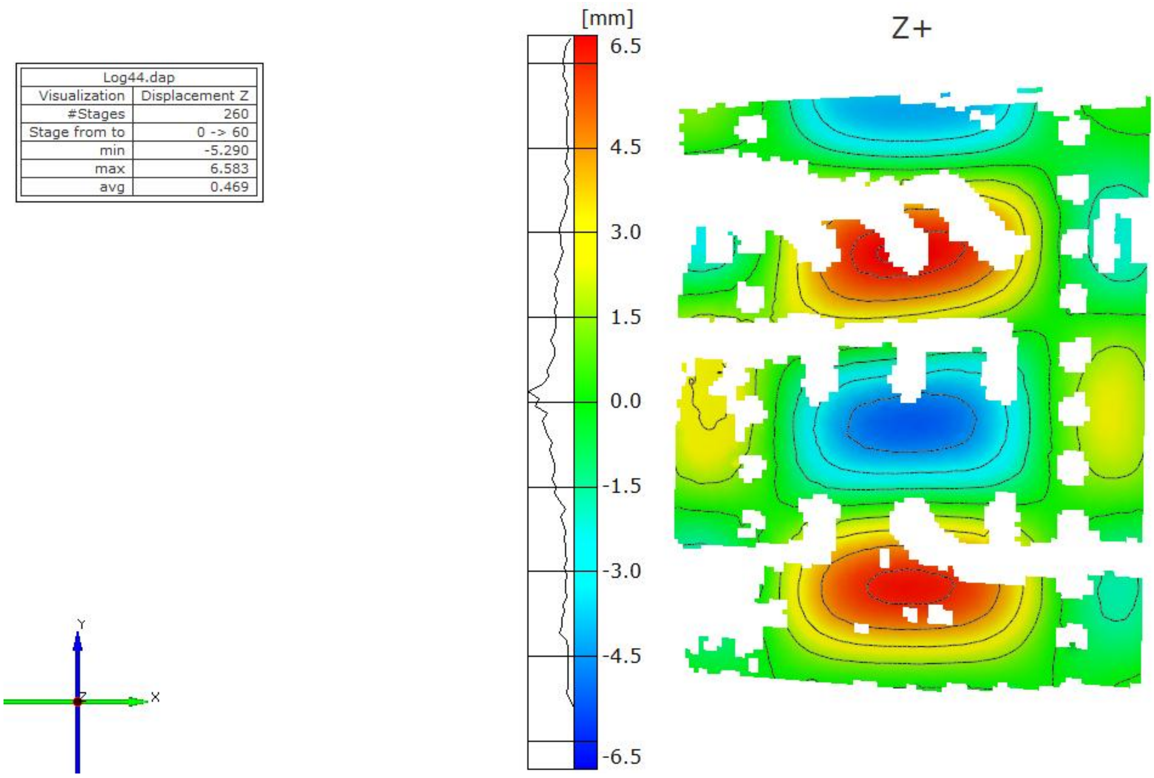

Fig. 3.11 Log 44 cycle 1, 298 s, 490 kN (Loading), Out of plane displ. range [-6.5,6.5] mm

The same measurements are shown in Fig. 3.12 and in Fig. 3.11 but with different scales to improve the resolution in the skin outside of the stringers. It may be seen that the maximum out of plane displacement outside of the stringers is about 0.75 mm bigger on the left hand side than on the right hand side.

The vertical displacement in cycle 1 of Log 44 is shown in Fig. 3.13. The displacement difference between the upper and lower edge of the region photographed by Aramis is here about 2.8 mm at 490 kN, over a length of about 400 mm, corresponding to a strain average of 0.7%. With a linear scaling to the full length of the panel the stroke would be 4.0 mm. This is within a few percent from the value that can be obtained from Fig. 3.2, presuming that the loading-curve can be shifted 0.65 mm to compensate for the initial nonlinearity in grip displacement.

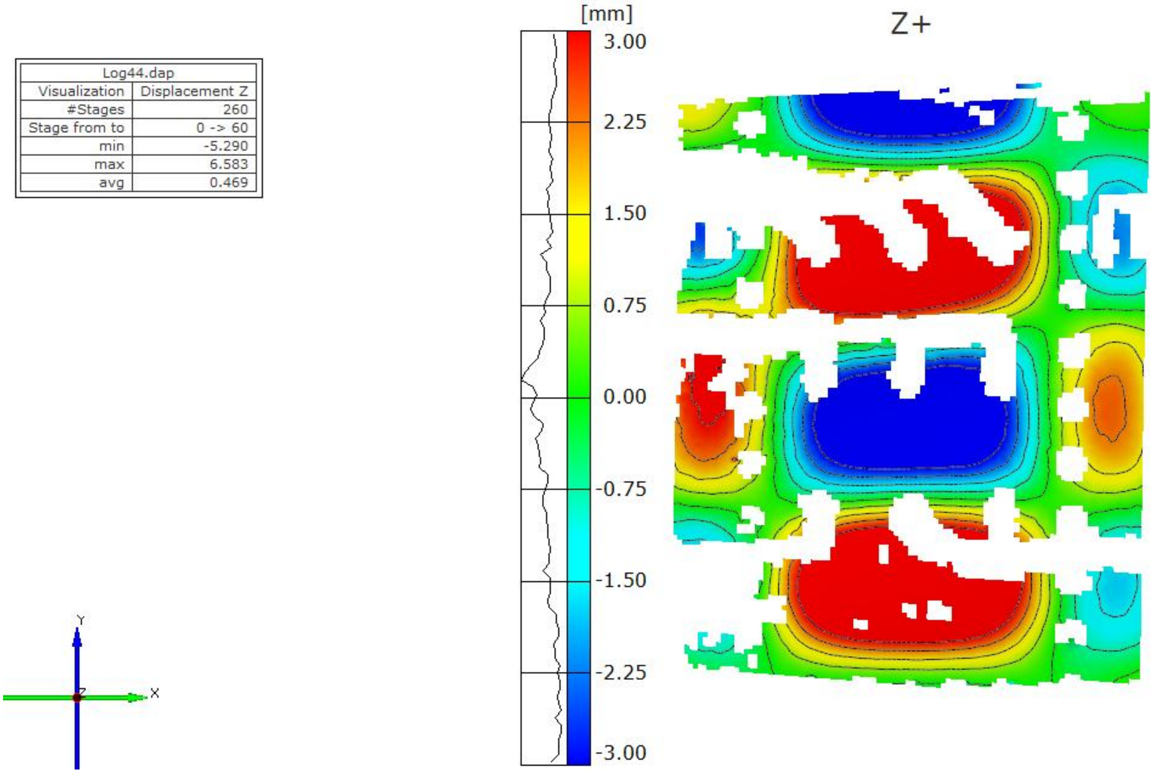

Figure. 3.12 Log 44 cycle 1, 298 s, 490 kN (Loading), Out of plane displ. range [-3.,+3.] mm

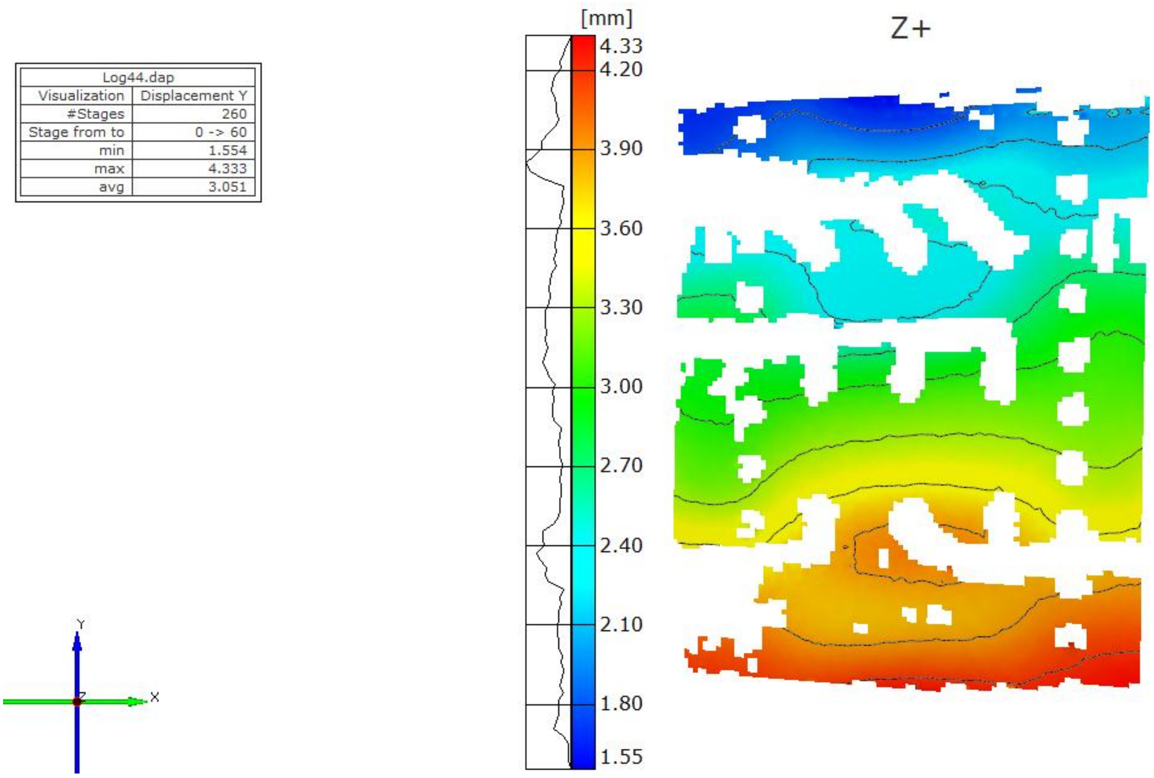

Figure. 3.13 Log 44 cycle 1, 298 s, 490 kN (Loading), vertical displacement

3.3 Strain gauge results

A total of 62 strain-gauges were attached as described in section 2.5. Compressive load and compressive strain are defined as positive in the discussion and in the graphs below!

In Fig 3.14 strains are shown for Log 31 cycle 1. For clarity the unloading part of the curves are shown only until 140 kN. No permanent strain was measured after complete unloading in this cycle. The panel and the loading-conditions are symmetric, the lay-up is symmetric and balanced, which should result in symmetries[2] in strain-data for gauges at equal distance to the lines of symmetry in the panel. The measured strain for gauge 14 and 16 as well as for gauge 6 and 18 are expected to coincide due to symmetry. However, it is seen that gauge 14 is strained faster initially, and gauge 16 more slowly than the gauges 6 and 18 below 30 kN. Below 80 kN the observations are similar for the corresponding gauges on the stringer-side of the panel. This indicate some unsymmetrical load-introduction, with the side closer to Y=0 being somewhat more loaded. In general the response for all gauges are nearly linear to about 100 kN with the first strain reversal occurring at 117 kN for gauges 6 and 36, followed by reversal at 128 kN for gauges 18, 35 and 37.

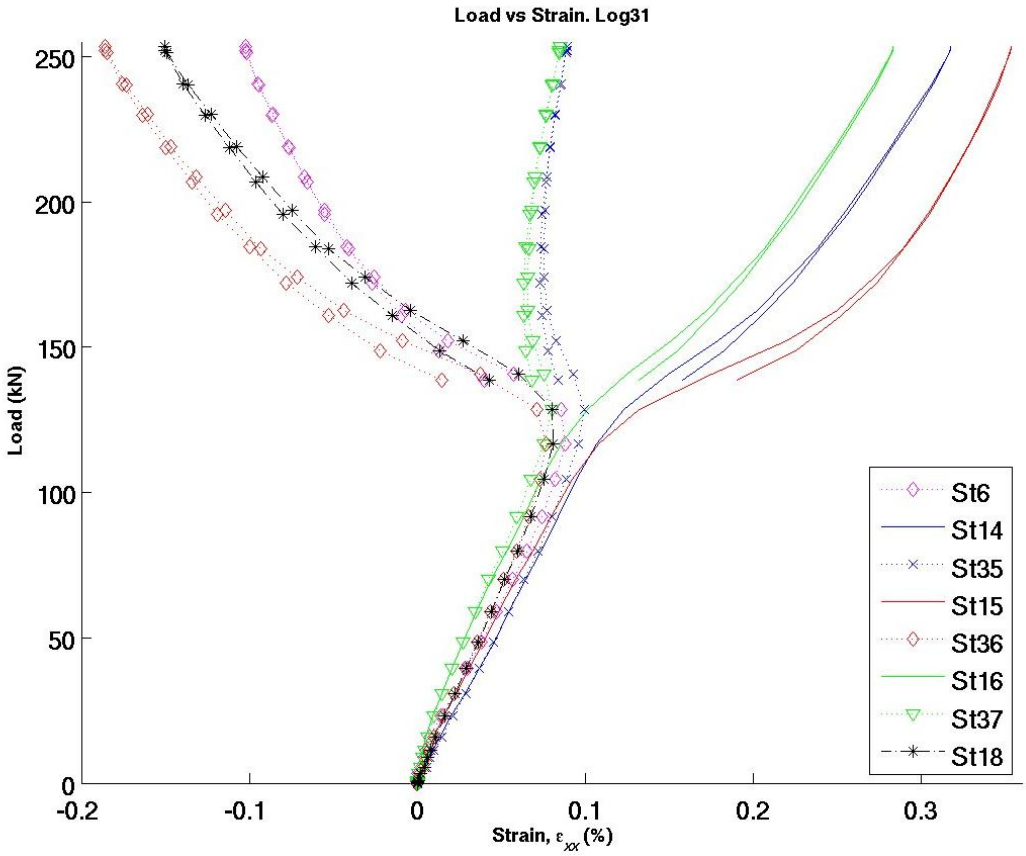

Figure 3.14 Strain in the loading direction for gauges on the skin

[2] Neglecting the influence of +/-45°-layer stacking on global symmetries

In the post-buckling regime gauges 6 and 18 are in fairly good agreement, as expected due to the symmetry in the panel at X=290. Gauge 36 on the stiffener side sense the highest tensile strain indicating that it is on the convex side of a buckle, which is also the case for the gauges 6 and 18 located directly above and below gauge 36, but located on the stiffener-free side of the panel.

The measured strains in the loading direction, for the gauges at X=190 on the stringer side, are shown in Fig. 3.15 during the two cycles in Log 35. It may be seen that the loading and unloading paths are slightly different, but cycle two follows cycle one closely. It is seen that the stringer at Y=100, with gauges 46 and 48 are more strained than the stringer at Y=300. It is also seen that the difference in strain between gauge 46 and 48 increase rapidly above 120 kN indicating stringer buckling, or wrinkling. This seems to be coupled with the buckling of the skin indicated by gauges 24, 27 and 30. The difference in response between gauges 50 and 52 on the other stringer is much smaller. Two gauges show discontinuities in their response indicating rapid change in buckling pattern, these gauges are No. 22 near a load of 140 kN and No. 34 near 350 kN. Data for gauge 2 showed large scatter and has been skipped, together with data for gauge 23 on the opposite side of the skin.

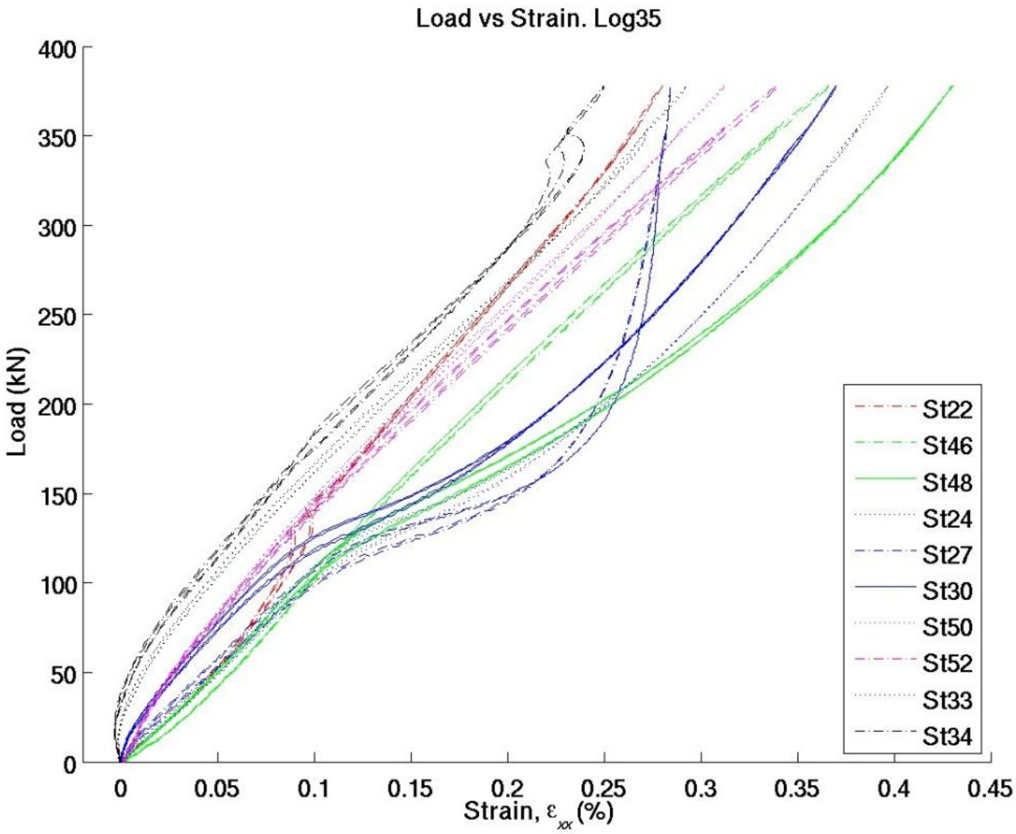

Figure 3.15 Strain in the loading direction, for the gauges at X=190 on the stringer side of the panel. Log 35

The two load-cycles in Log 35 are shown in Fig. 3.16. Looking for instance at the curve for gauge 15 it is seen that the loading and unloading paths are slightly different. The unloading-path are however practically identical between cycle one and two below 300 kN, showing no influence from the difference in maximum load (354 and 378 kN respectively).

The residual strain after cycle two is below 10 μStrain for the gauges shown, except for gauge 17 where a noise-level of about +/-40 μstrain blurs the reading. It thus seems that a single loading to 354 kN, which is three times above the load at strain reversal (buckling), can be applied without any registration of damage or permanent deformation.

The expected vertical and horizontal symmetries, for instance comparing the response of gauges 14 and 16 or 6 and 18, exist also for the highest load-levels.

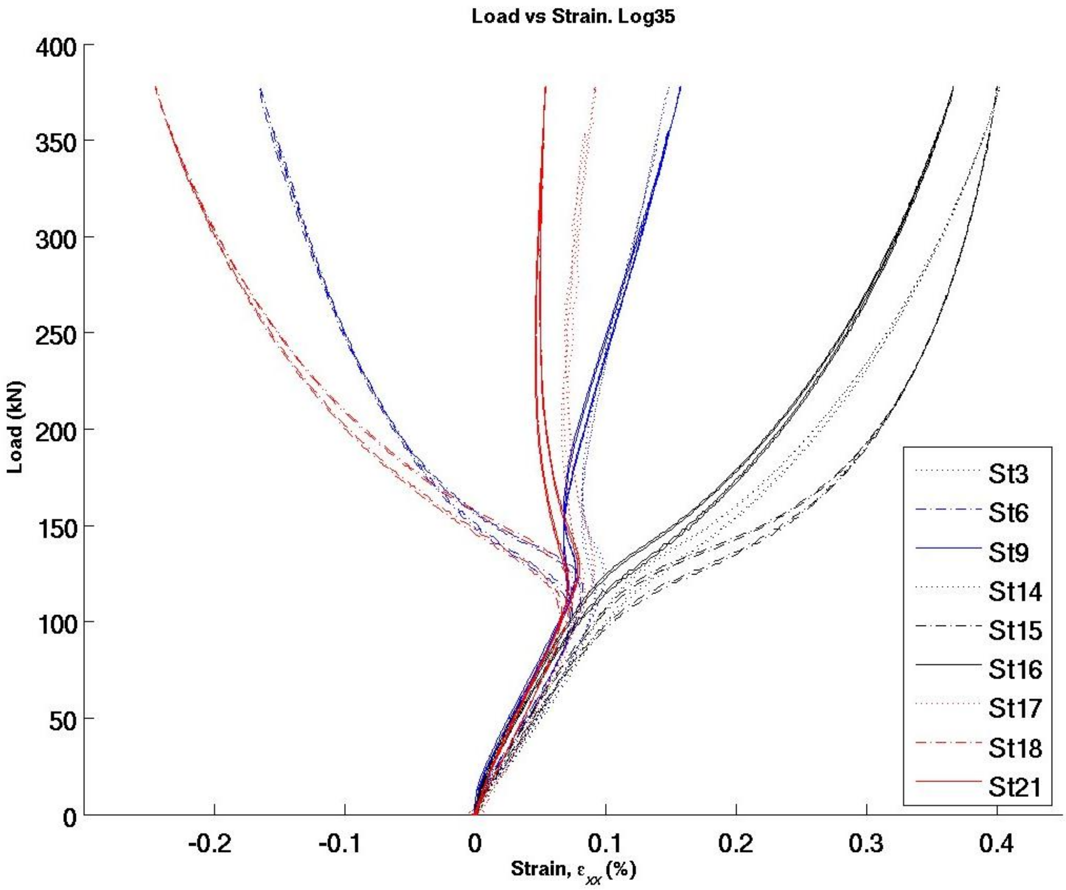

Figure 3.16 Strain in the loading direction for gauges on the stringer-free side of the skin. Log 35

In Log 38 there is a visible difference in the path between the first and the second cycle for gauges 3,6, 9 and 17 as may be seen in Fig. 3.17. There might also be some residual strain in the rather noisy signal from gauge 17. The behaviour of bolts can be expected to be rather non-linear due to contact and friction. This may influence the strain at nearby gauges.

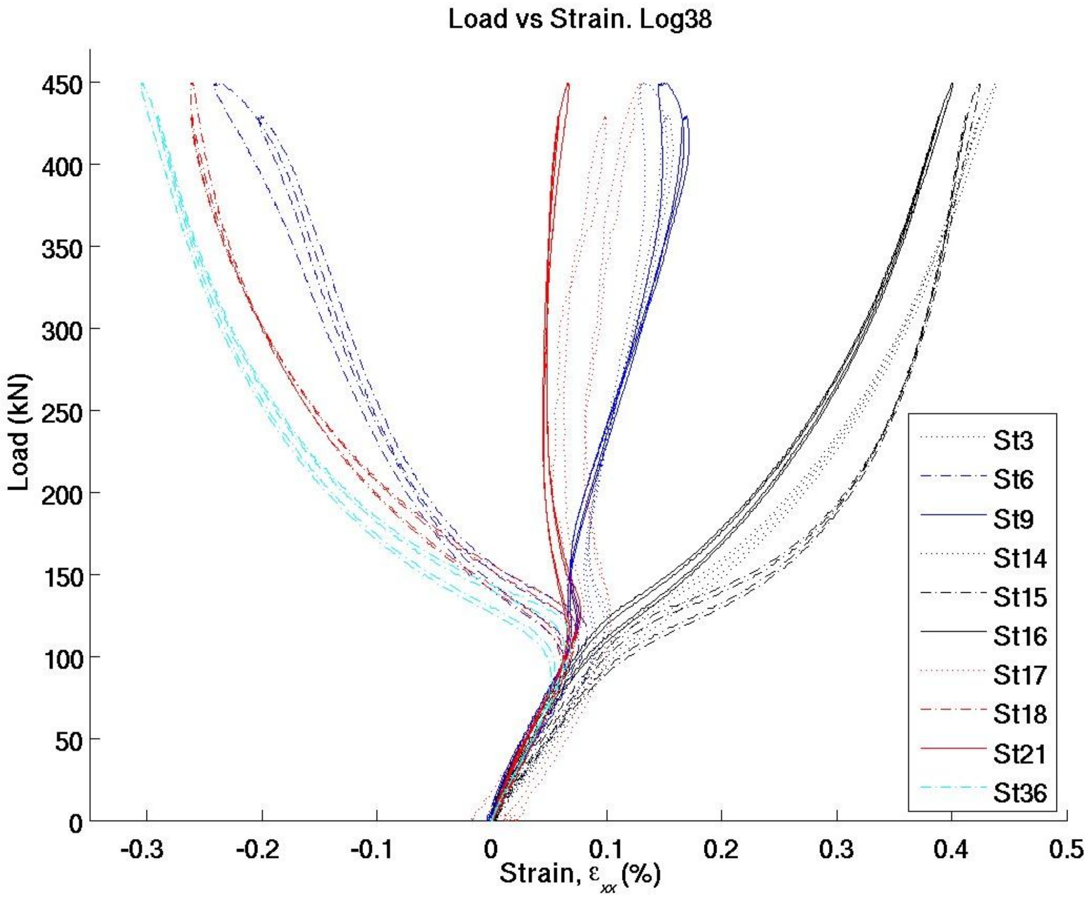

Figure 3.17 Strain in the loading direction for gauges on the stringer-free side of the skin, and also for gauge 36 in the middle of the stringer-side. Log 38

The response in Log 40 is shown in Fig. 3.18. Compared to previous cycles the difference in strain response is in general larger in Log 40 between the paths in cycle one and two. It is also seen that gauge 9 has significantly different unloading-paths in the two cycles. Some residual strain is observed for gauge 14 in the second cycle.

Gauge 6 seems to give in when reaching 460 kN in cycle two. The signal suddenly corresponds to the limit set by the amplifier (4% tensile strain), but for some reason the gauge recovers again below 350 kN.

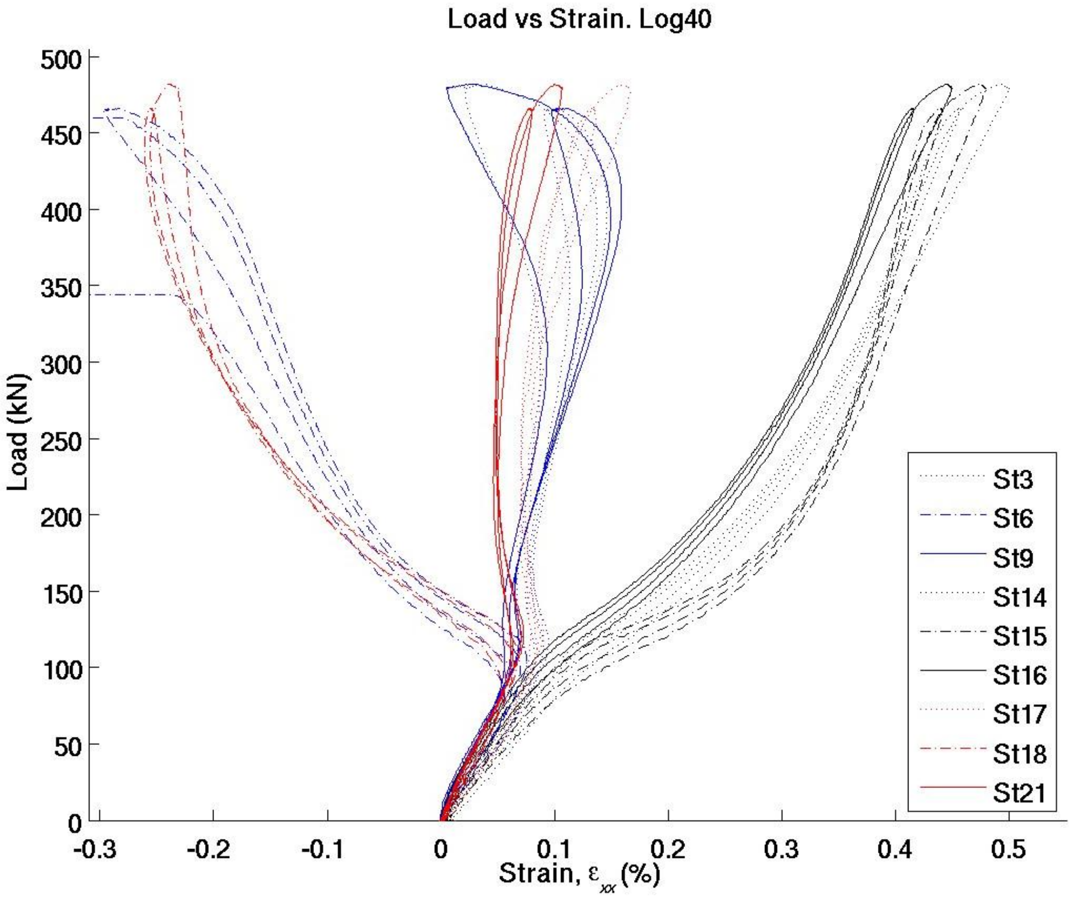

Figure 3.18 Strain in the loading direction for gauges on the stringer-free side of the skin. Log 40

The strain response in Log 42 is shown in Fig. 3.19. Most strain-gauges now show significantly different paths in cycle one and two, and significant residual strains. The difference in strain between gauge 14 and 16 near maximum load becomes much higher in cycle two where the maximum compressive strain in gauge 14 is 0.68%. A strong discontinuous behaviour is again observed for gauge 6.

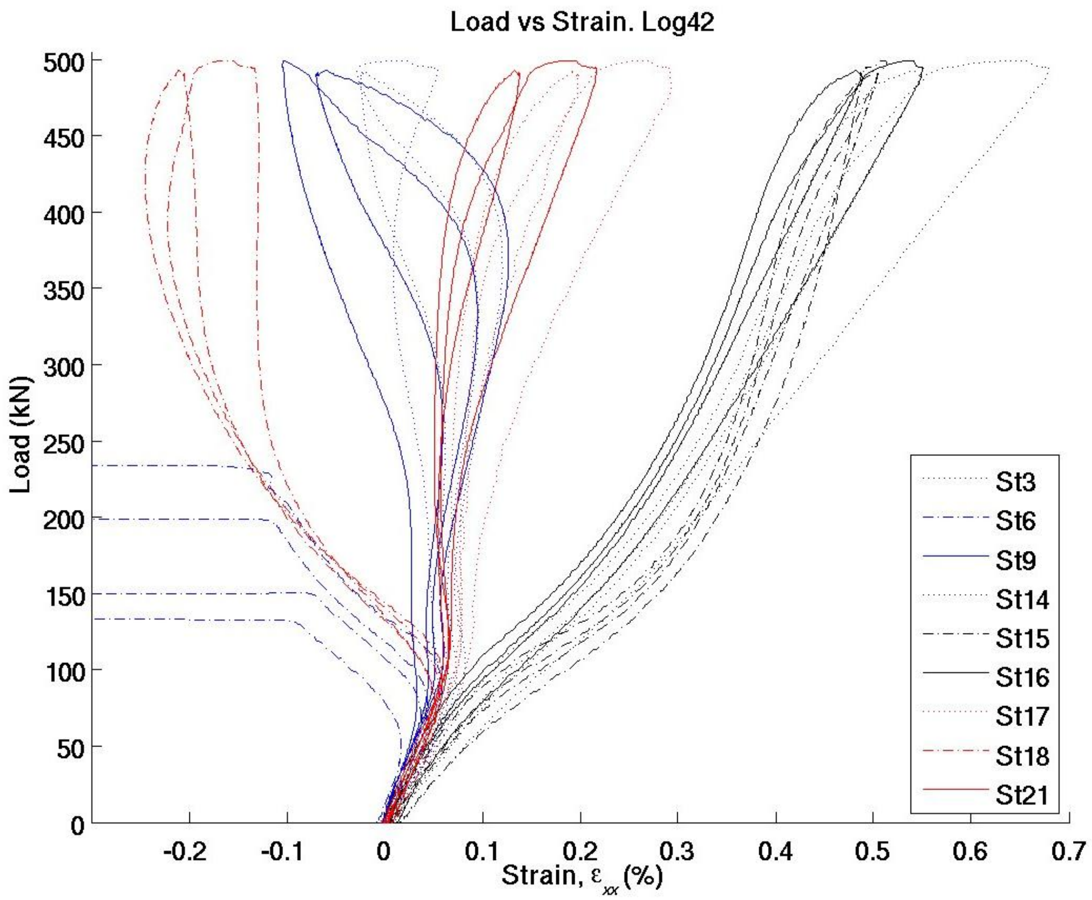

Figure 3.19 Strain in the loading direction for gauges on the stringer-free side of the skin. Log 42

The response in Log 44 is probably influenced by the plastic deformation and/or damage occurring during previous and the present cycle as shown in Fig. 3.20. Looking for instance at gauges 14 and 16 at a load of 400 kN. The strain difference is about 450 μStrain between the loading paths for cycle 2 in Log 42 and that in Log 44. In the unloading-paths for Log 44 there are straight lines from about 486 kN to 250 kN which just indicates that the unloading was so rapid (while the stroke is slowly changing) that there are no intermediate registration of strain. If the panel has any residual strength it seems to be at most 250 kN. No additional load-cycles were performed and it is possible that further damage growth in such event would reduce the residual strength to even lower values.

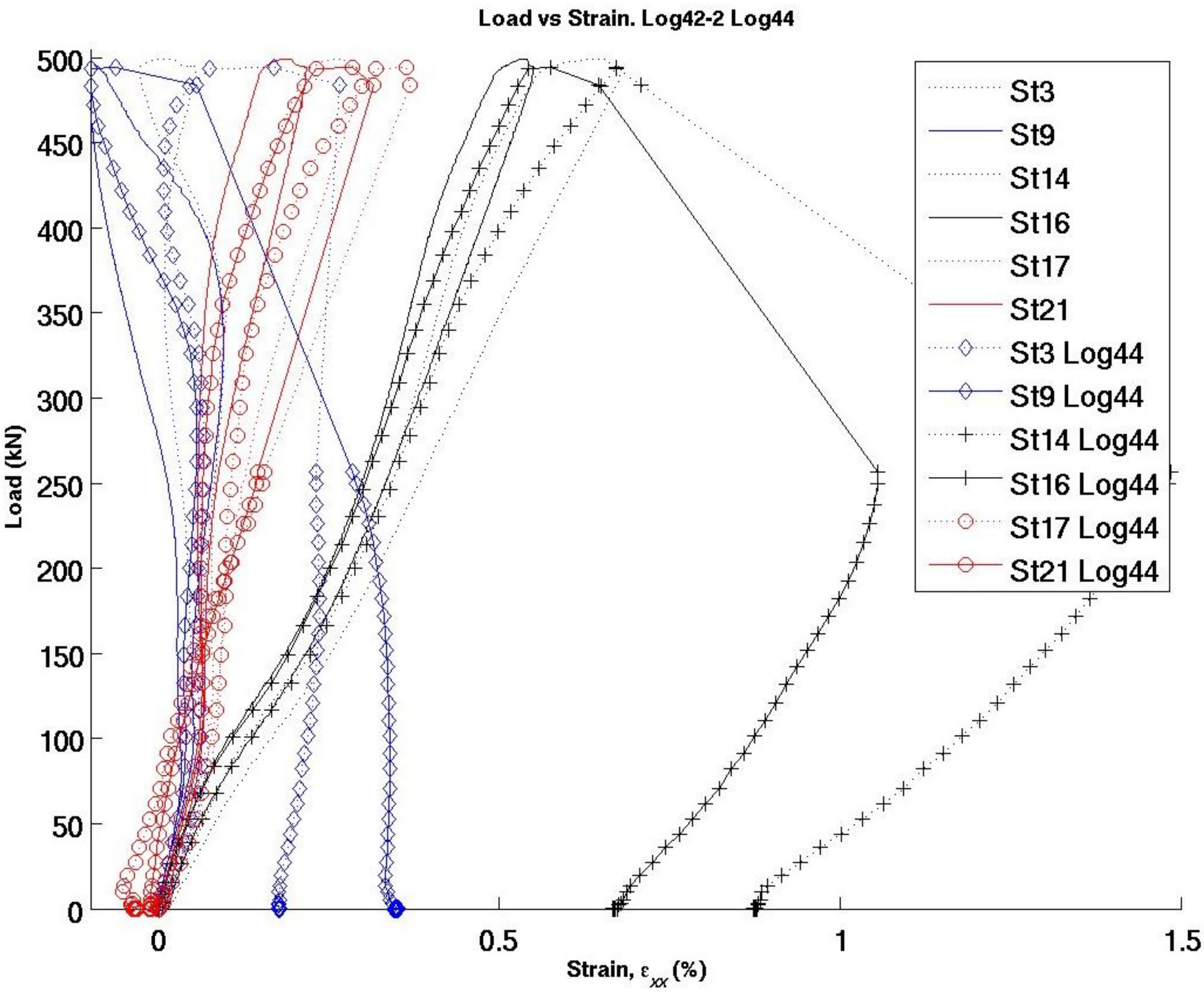

Figure 3.20 Strain in the loading direction for gauges on the stringer-free side of the skin. Log 42 cycle 2 and Log 44 including collapse

The strain in the row at Y=190 will be discussed below. Data for gauge 2 showed large scatter and has been skipped, together with data for gauge 23 on the opposite side of the panel.
The strain registration in the loading part of Log 38 cycle 1 is shown in Figs. 3.21 & 3.22, where the latter is showing the response up to maximum load for Log 38. It is seen also here that the side around the stringer at Y=100 is initially more strained than the side around the stringer at Y=300. The difference in strain between gauge 1 and 13 at 100 kN is 620 μStrain.

The curves indicate buckling of the skin between the stringers (gauges 3, 6, 9, 24, 27, 30) near 120 kN. Gauges 1 and 22 (at Y=30) indicate a possible change in buckling pattern near 140 kN, at least locally.

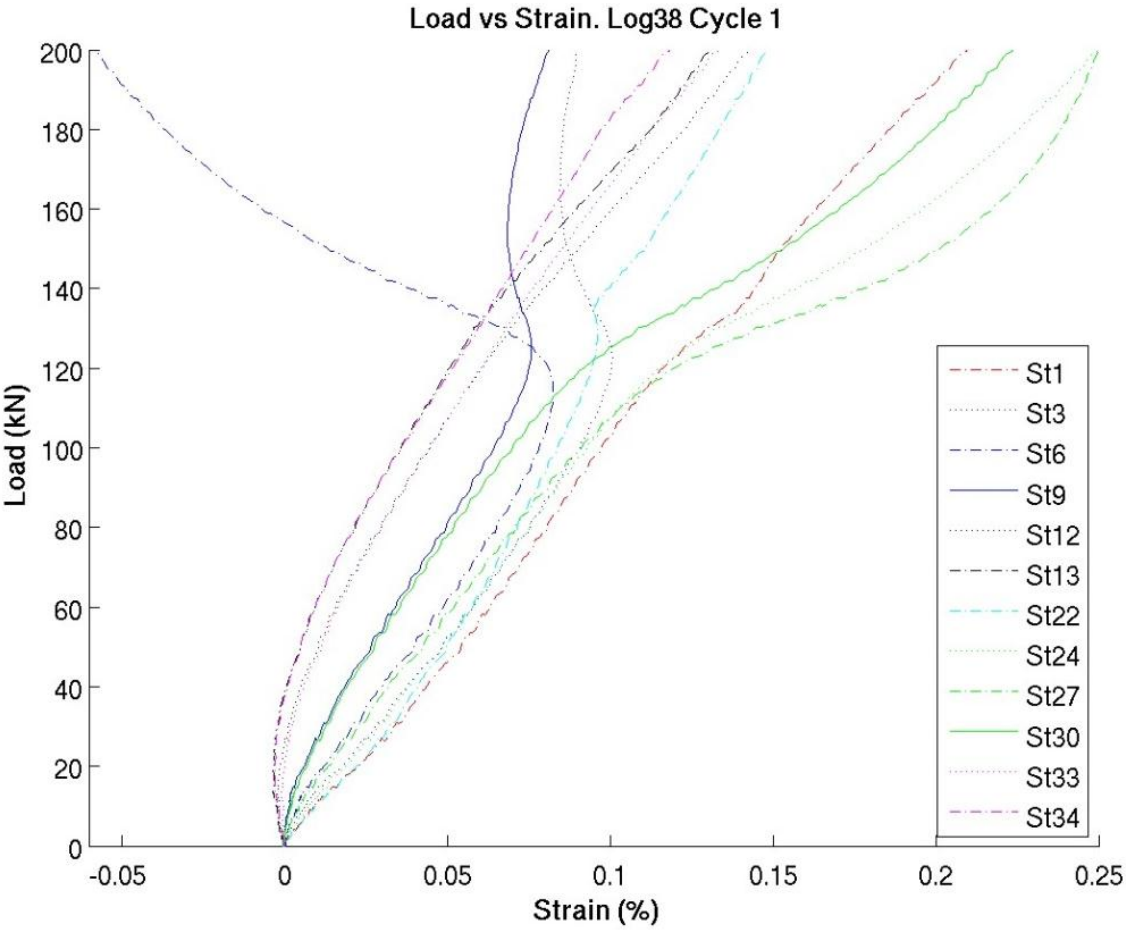

Figure 3.21 Strain in the loading direction for gauges at X=190 on both faces of the skin. Log 38 part of loading in cycle 1

In Fig. 3.22 it is seen that the gauge subject to the highest compressive strain at loads above 330 kN is gauge 1 reaching 0.52%. Some change in buckling pattern is indicated at 350 kN by the strain-gauge pair 13/34, with an increase in compressive strain for gauge 13, and a decrease for gauge 34.

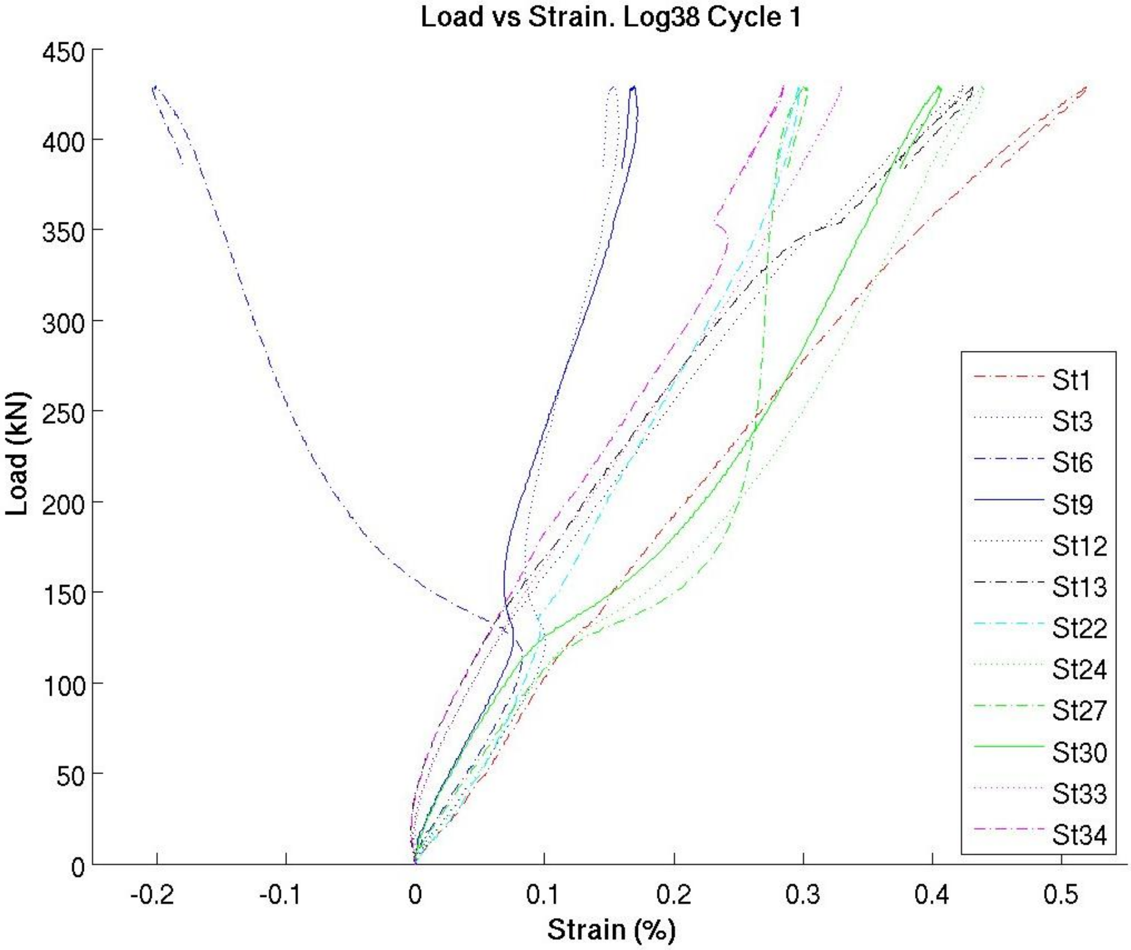

Figure 3.22 Strain in the loading direction for gauges at X=190 on both faces of the skin. Log 38 cycle 1 to maximum load

The average, or membrane strain, for pairs of gauges on opposite sides of the panel is shown in Fig. 3.23. It seems that the stringer at Y=100 carries a substantially higher load than the stringer at Y=300. It is also seen that the middle of the panel does not carry its share of the load, in proportion to the totally applied load at loads above about 140 kN.

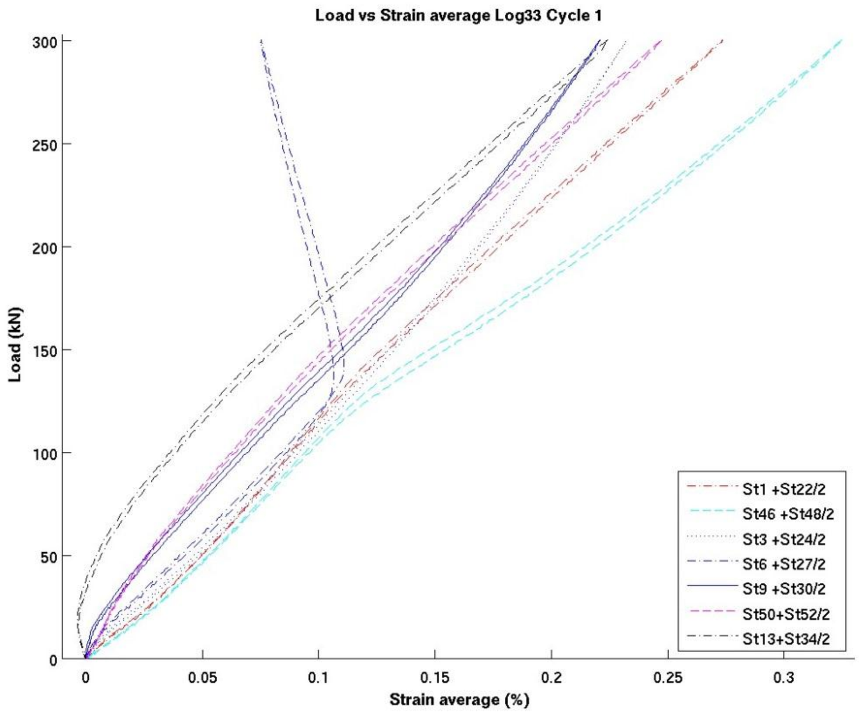

Figure 3.23 Average strain in pair of gauges at X=190. Log 33 cycle one

The strain difference between points at opposite sides of the skin and stringers are shown in Fig. 3.24 for the first cycle in Log 33. It may be seen that some bending is introduced into the stringer at Y=100 (gauges 46&48) from the onset of loading.

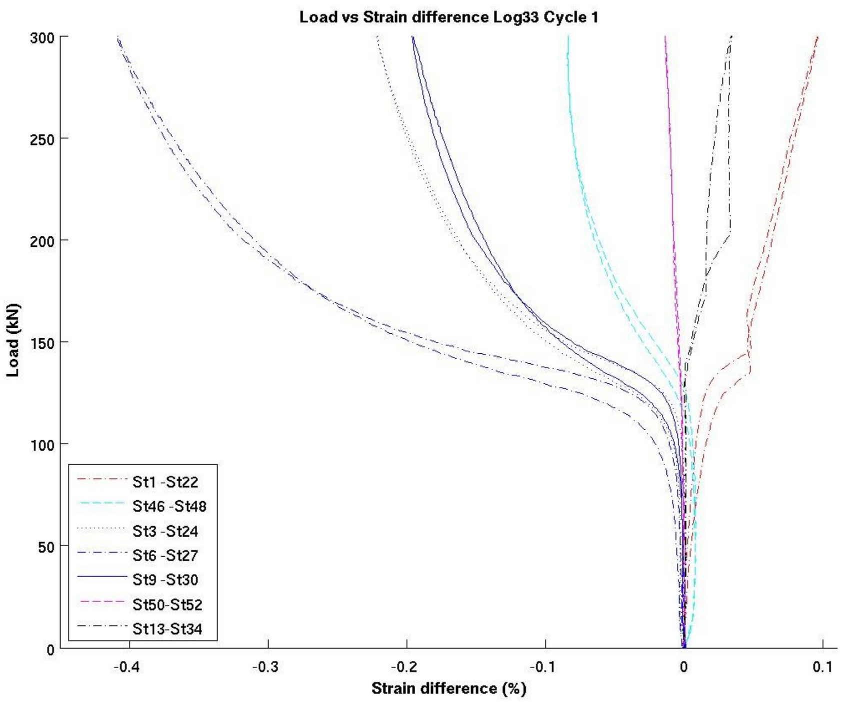

Figure 3.24 Strain difference (bending strain) in pair of gauges at X=190

The curves in Figure 3.25 show the response as the average of gauges 1, 13, 22 and 34 from the Logs:26,33,38 and 42. The curves are not even very linear below 100 kN in the first Logs, and the curves are clearly non-linear above 100 kN.

There is some residual strain after the first cycle in Log 42, but it becomes more easily visible after the second cycle. It should be mentioned that all strain-gauges are calibrated to zero strain at zero load before each Log is started.

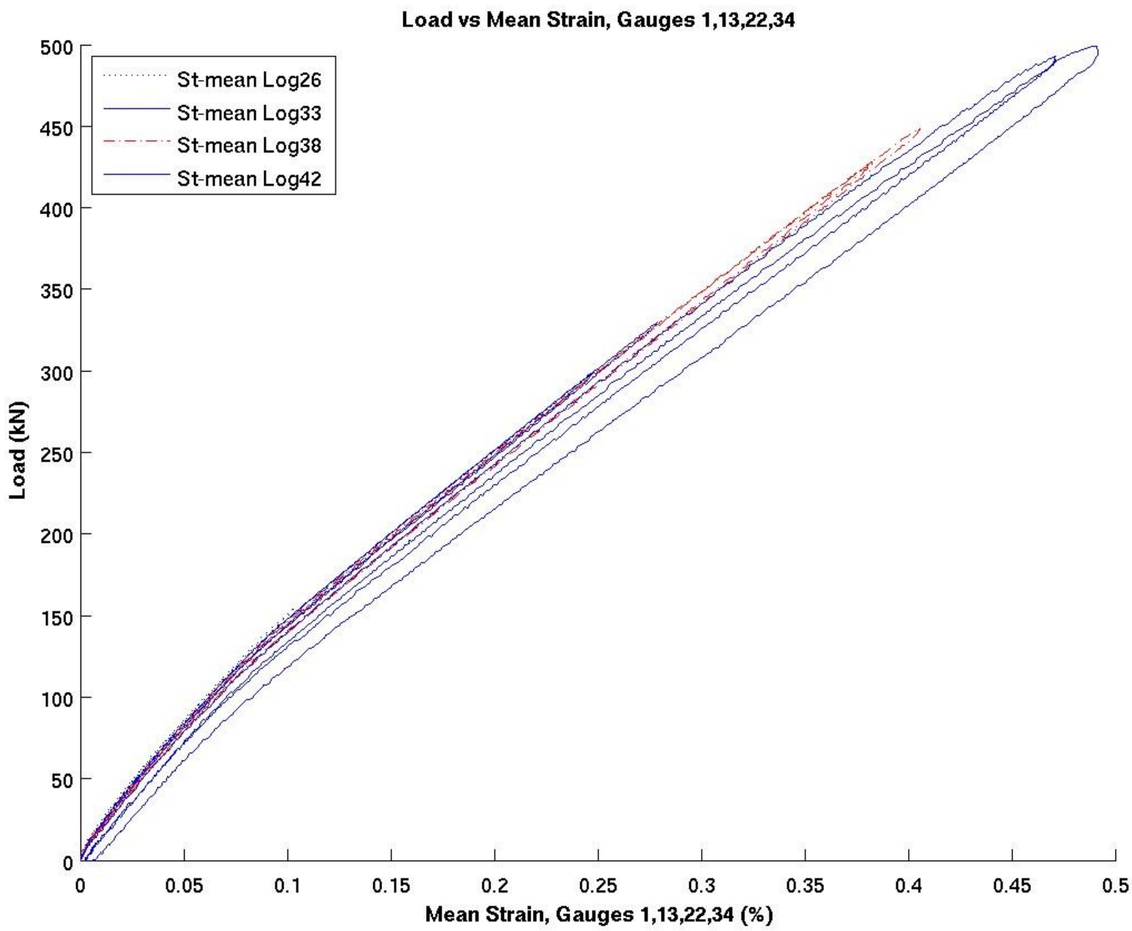

Figure 3.25 Average strain response for gauges 1,13,22 and 34 in cycles to different maximum load

In Figure 3.26 below the curves from Figure 3.25 is multiplied with panel length (580 mm) giving an estimate of the stroke. This stroke estimate, approximately 2.1 mm at 400 kN in Log 38 is fairly close to the estimate based on Aramis results (2.3 mm) discussed in association with Fig. 3.8.

Similarly using strain gives a stroke estimate of 2.85 mm at maximum load in Log 42 (499 kN) gives however a much lower value than the grip displacement in Table 2.2, which was 4.8 mm. Even if this value is reduced by 0.65 mm to compensate for initial nonlinearities in the test-setup the difference is still large, being 1.3 mm.

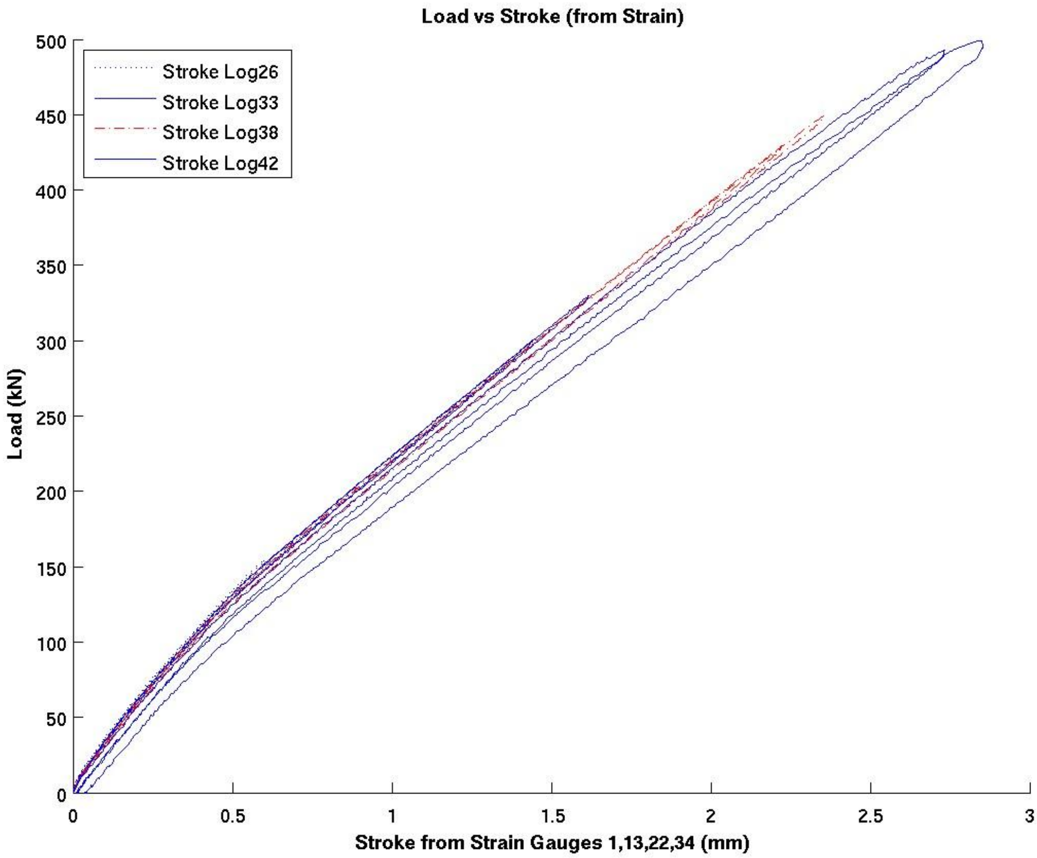

Figure 3.26 Stroke estimate predicted from average strain for gauges 1, 13, 22 and 34, in cycles to different maximum load

Below are curves for four pairs of rosette-gauges with the response shown for the loading part of the first cycle in Log 38.

When comparing the green curves between Fig. 3.27 and 3.28 it must be remembered that they should be different, since the 45^{o}-direction is anti-symmetric *wrt.* the vertical plane at Y=200. The other curves show in general a fairly good correlation, indicating some symmetry in the general behaviour.

There is for some unknown reason something strange with the reading from gauge 40 in Fig. 3.30.

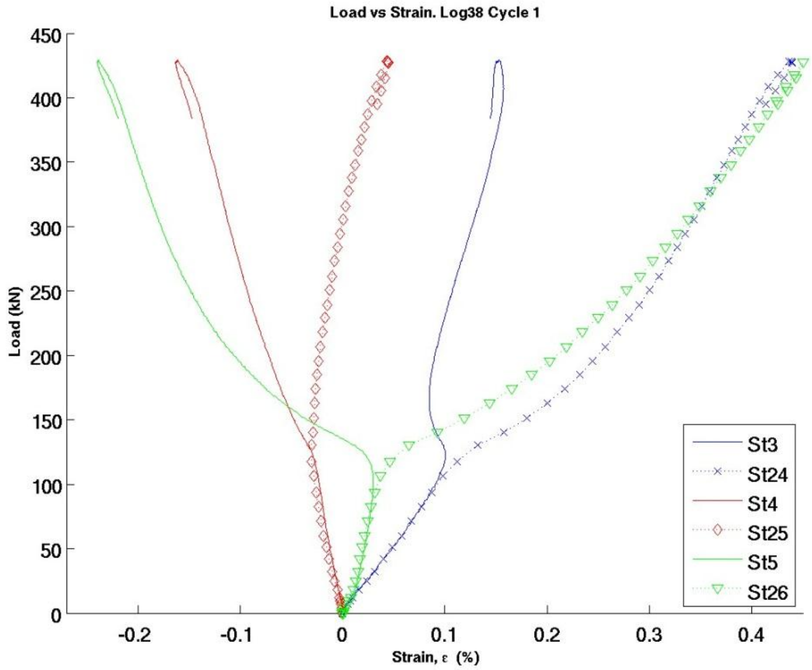

Figure 3.27 Strain in the rosette at X=190 and Y=133

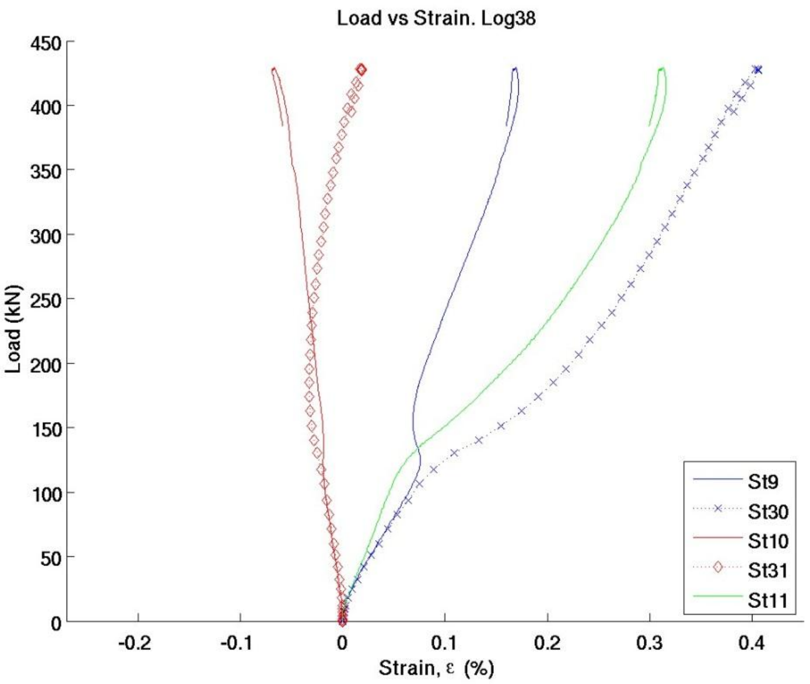

Figure 3.28 Strain in the rosette at X=190 and Y=266 (Gauge 32 was not responding)

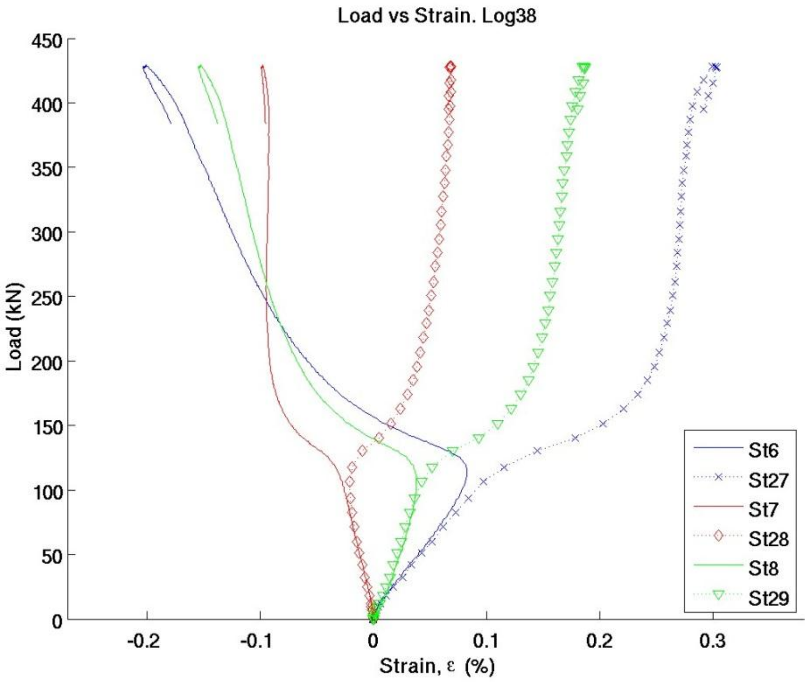

Figure 3.29 Strain in the rosette at X=190 and Y=200

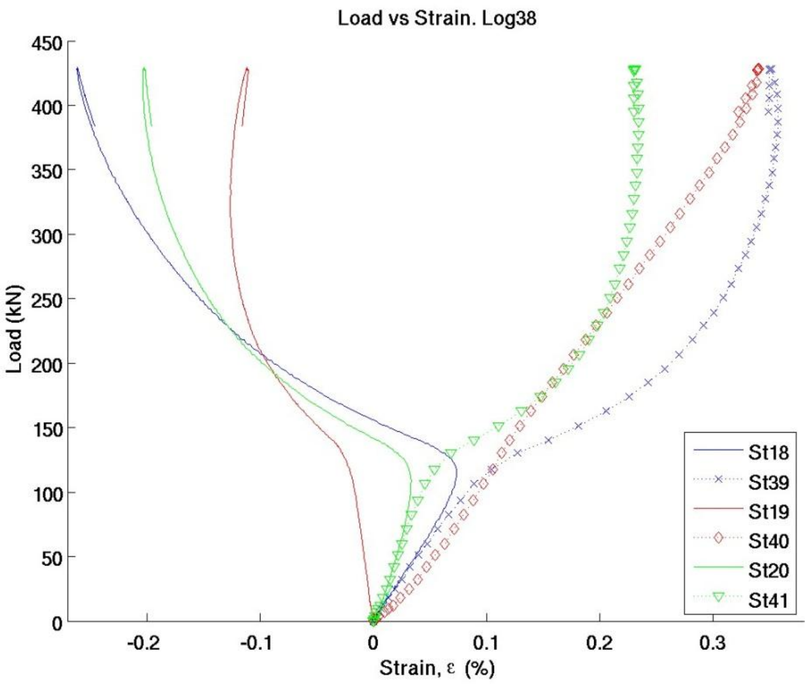

Figure 3.30 Strain in the rosette at X=390 and Y=200 (Response from gauge 40 is strange)

The symmetry in strain response *wrt.* Y=200 can be seen for gauges 25 and 31 measuring strain in the y-direction when studying Fig. 3.31. Gauges 24 and 30 lose that symmetry near maximum load in the second cycle. Gauges 28 and 40 behave completely different indicating differences between the upper and lower part of the panel in Log 42. The signal from gauge 38 was too noisy to be useful.

Gauge 40 indicates significant residual strains already after the first cycle, and gauge 24 is also measuring significant residual strains after the second cycle.

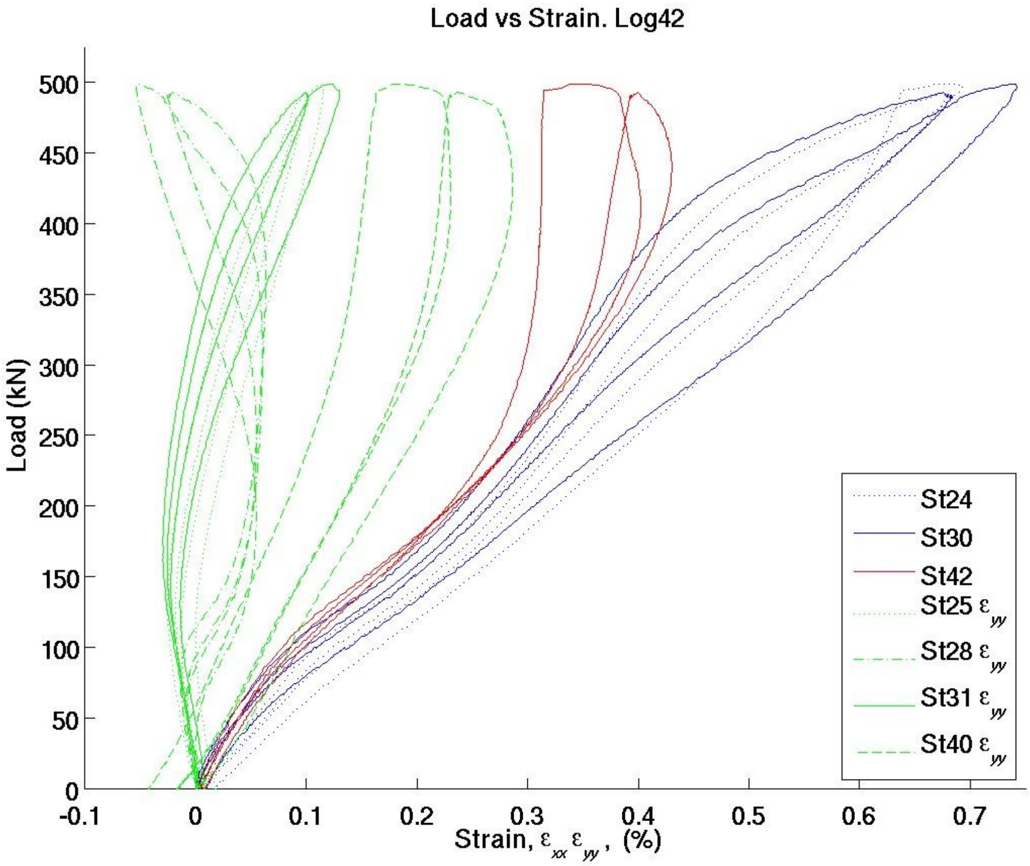

Figure 3.31 Strain in rosettes during Log 42

The tensile z-direction strain in the stringers, near their root, is shown in Fig. 4.19.

In Fig. 3.24 it was shown that the compressive strain for gauge 1 is about 0.7% at loads close to 500 kN. With a Poisons ratio of 0.3 for the aluminium stringer, and assuming similar axial strains as for gauge 1, we can expect a tensile strain of 0.21% in the Z-direction due to the axial loading. The tensile strains in Fig. 3.32 are similar in magnitude at high load-levels, making it hard to draw any conclusion concerning separating forces (peeling) between skin and stringers.

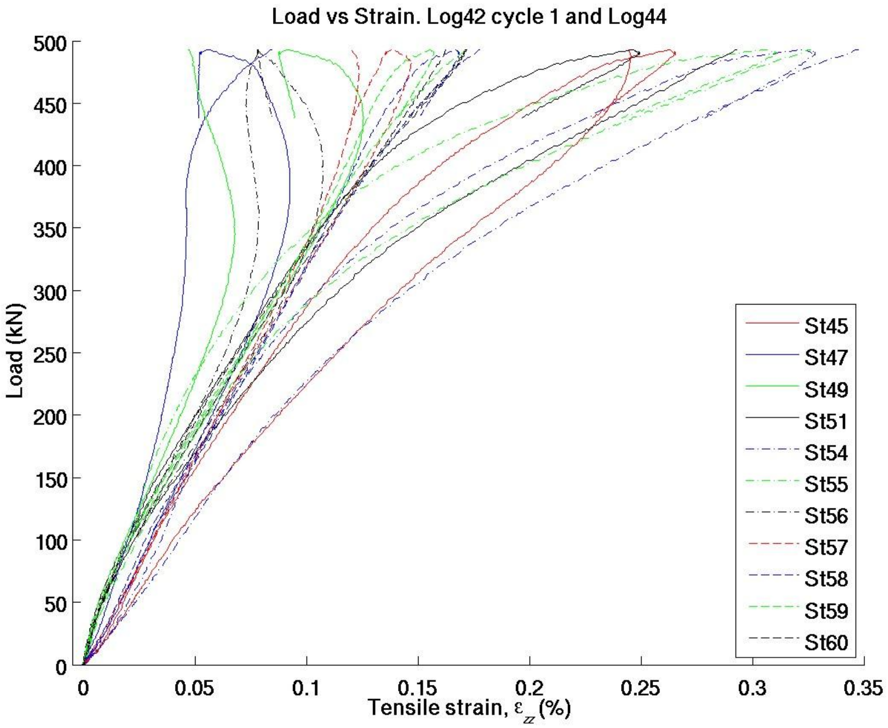

Figure 3.32 Tensile z-direction strain in the stringers, near their root

The average tensile z-direction strain in the left and right stringer is shown in Fig. 3.33. There is a significant strain increase at the location of gauges 55/56 when the maximum load is reached.

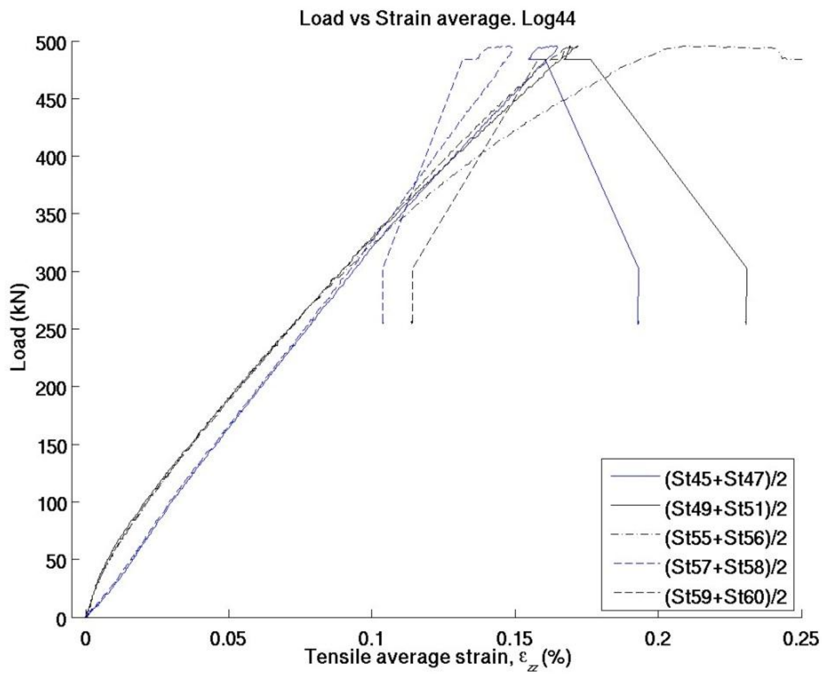

Figure 3.33 Average tensile z-direction strain in stringers

The strain difference (bending strain), in the z-direction in the stringers is shown in Fig. 3.34, for the loading and first part of unloading in Log 44. The pair 45/47 indicates bending from the onset of loading. Gauges 55/56 and 49/51 indicating more than 0.1% bending strain beyond 375 kN, and the bending strains increase until maximum load where it reaches +/-0.32%. The collapse is very rapid with only one registration at about 480 kN, followed by the next at 300 kN and a third at 255 kN.

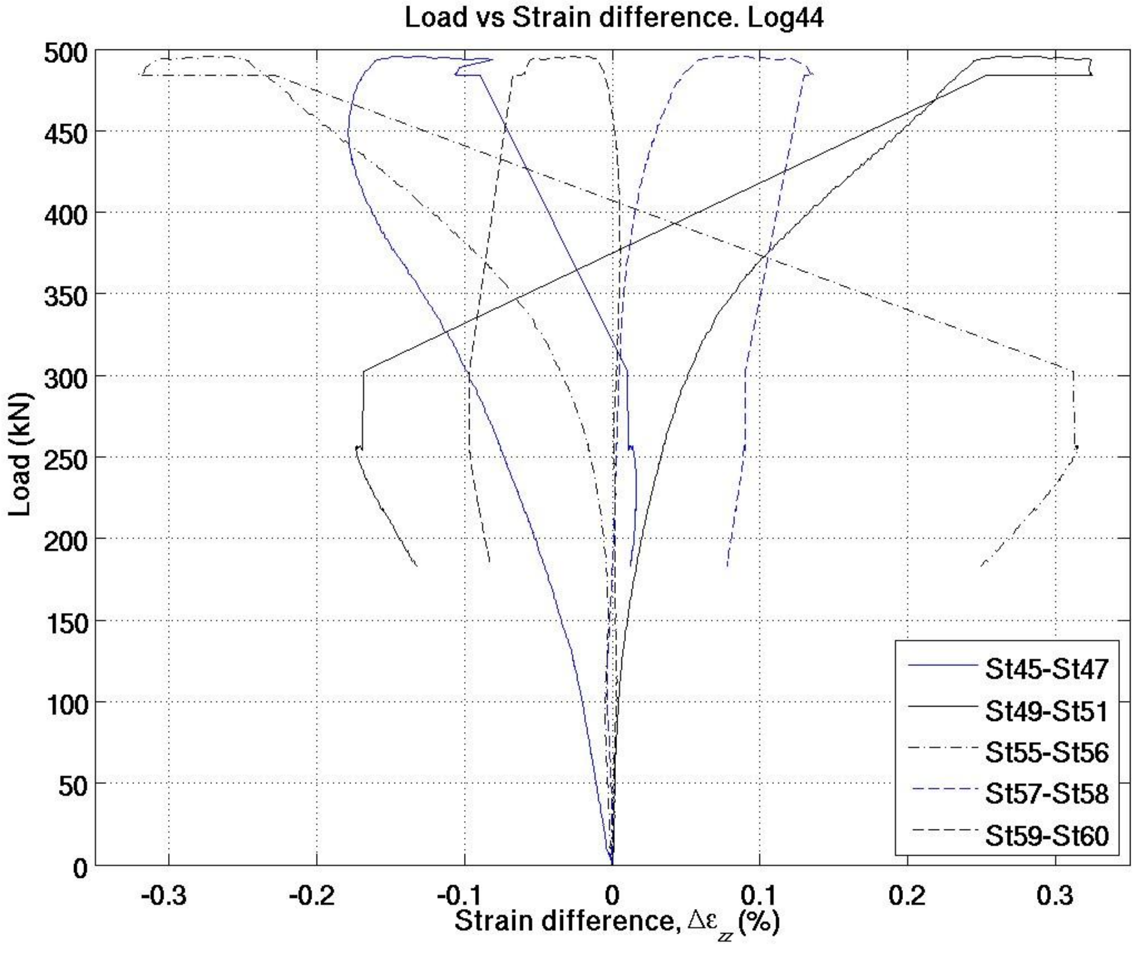

Figure 3.34 Bending strain in stringers near stringer web root

For completeness the strains in the two short horizontal stiffeners (Frame or spar foot) are shown for Log 42 in Fig. 3.35. Gauge 43 seems to be out-of-order and the levels for the other gauges are very small.

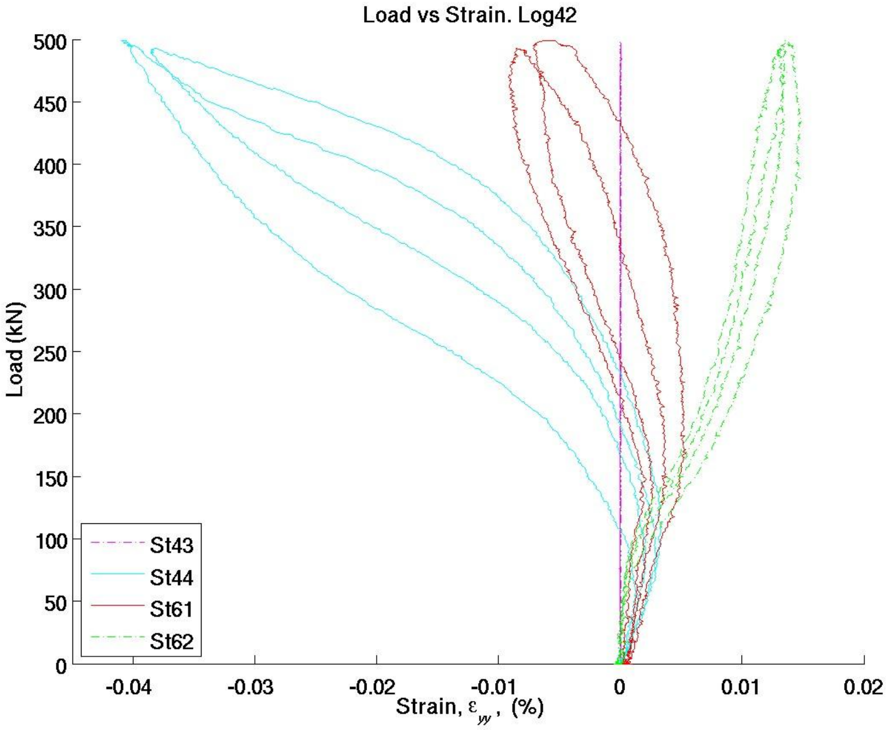

Figure 3.35 Strain in the two short horizontal stiffeners (Frame or spar foot)

3.4 Residual strain

Strain-gauges 10 and 17 indicate the largest residual strain of all gauges after Log 35 with 21 and 39 μStrain respectively. The signal from gauge 17 is somewhat noisy, and it's not clear if is an effect of the panel behaviour or caused by the measurement system.

There are three gauges measuring residual strains higher than 30 μStrain after Log 38. The gages are No. 6, 14 and 17 with the values 37, 33 and 388 μStrain.

The signal from gauges 2, 23,38 and 53 were so noisy already in Log 35 that they were not taken into account.

3.5 Effective width calculation

The load distribution between the stringers and the left, centre and right part of the skin can be estimated with help of the diagram in Fig. 3.23, and the stiffness properties given by Tab.2.1. The so called effective load-carrying width of the skin between the stringers at loads beyond the buckling load can also be estimated.

Manually reading the strain in the diagram one may obtain for the different parts where the gauges are located
[Skin Stringer skin skin skin Stringer skin]
the strains at 125 kN:
[0.1059 0.1147 0.1088 0.1029 0.08823 0.08235 0.05882]*0.01
and similarly at 250 kN:
[0.2118 0.2559 0.1912 0.08529 0.1794 0.1882 0.16471]*0.01

Calculating the stiffness (width*thickness*Elastic modulus) representative for each part one obtains:
[19. 29.5 37.9/3. 37.9/3. 37.9/3. 29.5 19.]*10^6
A simple multiplication gives: 127.3 and 260.1 kN, indicating a slight over-estimation. Similarly, using only the three values in the middle of each vector, representing the load carried by the skin between the stringers, one obtains 37.9 and 57.6 kN.
The effective width, B_{eff}, at a load of 250 kN, with correction for the slight overestimation of total load is now calculated as:
B_{eff}/B=57.6*/(37.9*(260.1/127.3))=0.74=74% of the width at 125 kN.

With support from the straightness of the curve for the gauges at Y=201 up to 125 kN in Fig. 3.23 it may be assumed that the skin is 100% effective at that load.

3.6 Post mortem

Pictures of the failed specimen after it had been removed from grips are shown in Figs. 3.36 and 3.37. A compressive failure occurred across the width of the specimen close to the centre of the specimen and not in the vicinity of where the load was introduced. The vertical stringers show large permanent deformation where failure occurred. On the smooth side of the panel it is hard to see the failure due to poor contrast and the speckle paint.

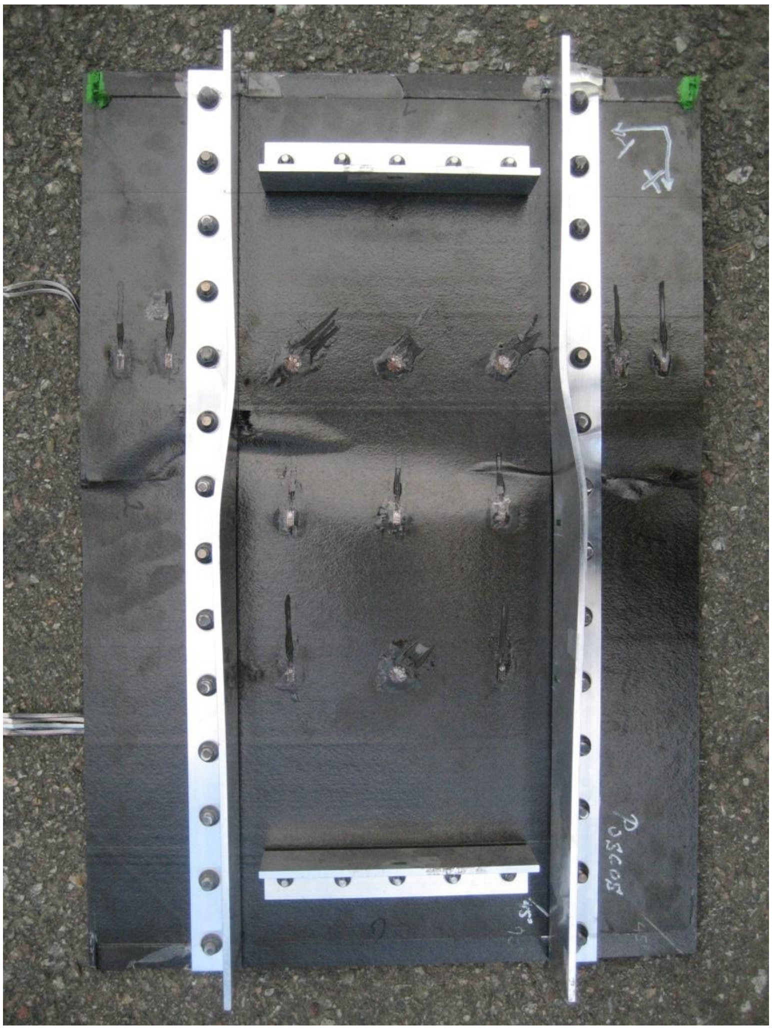

Figure. 3.36 Specimen after testing. Picture showing collapse, including complete failure across the skin and permanent deformation of the aluminium stringers

Figure. 3.37 Specimen after testing, showing compressive failure across the composite skin

4 Summary and Conclusions

A hybrid aluminium-composite structure has been tested in compression to failure to study the effect of buckling. The buckling displacement shape was registered with optical technique (ARAMIS). A total of 62 strain-gauges were used to record detailed strains in the specimen. Failure occurred in the measurement area.

Strain reversal was observed at 117 kN and the panel has been loaded to successively higher loads 14 times before the first indication of possible damage occurred at a load being more than three times higher. It seems that a single loading to 354 kN, which is three times above the load at strain reversal (buckling), can be applied without any registration of damage or permanent deformation.

The collapse at 495 kN was very sudden after reaching 499 kN in the previous load cycle with some acoustic noise being heard indicating damage growth. A significantly lower residual strength was indicated by the rapid load reduction, with no intermediate readings of strains between the maximum load and 300 kN. Visual inspection of the panel revealed damage across the skin from one side to the other.

It should perhaps be remarked that by design there is a central part of the panel between the stringers that is prone to buckling and a surrounding region with the stiffeners which is fairly well supported by the test-rig. This panel design with the boundary conditions applied can as shown give very high collapse loads. Conditions where the stiffeners are less supported can be expected to show a lower ratio between collapse load and buckling load.

The test has shown that the load-carrying capacity of the panel is significantly higher than the buckling load for the skin. It has also been shown that a few load-cycles with maximum amplitudes much higher than the buckling load can be applied without causing damage to the panel.

FOI
Defence Research Agency
SE-164 90 Stockholm

Phone: +46 8 555 030 00
Fax: +46 8 555 031 00

www.foi.se